

**Non-linear Slip-Based Brake Control and Accompanying Road Force
Observation**

by

Richard Charles Hill

B.S. University of Southern California, 1998

Submitted in partial satisfaction of the
requirements for the degree of
Master of Science

in

Mechanical Engineering

in the

GRADUATE DIVISION

of the

UNIVERSITY of CALIFORNIA at BERKELEY

Committee in charge:

Professor J. Karl Hedrick, Chair
Professor Masayoshi Tomizuka

2000

Contents

List of Figures	iv
1 Introduction	1
1.1 PATH AHS Concept	1
1.2 PATH AHS Program Status	3
1.3 Motivation and Goals	4
2 Control Model	9
2.1 Vehicle Dynamics	9
2.2 Wheel Dynamics	9
2.2.1 Brake Torque	10
2.2.2 Shaft Torque	11
2.3 Tire Model	11
3 Slip Based Dynamic Surface Controller	13
3.1 State Equations	13
3.2 Controllability	14
3.3 Dynamic Surface Controller	15
3.3.1 Controller Design	15
3.3.2 Benchmark Controller	17
3.3.3 Nominal Simulations	18
3.3.4 Robustness Simulations	19
3.3.5 Contribution of the Limited Slip Assumption	21
3.4 Adaptive Dynamic Surface Controller	22
3.4.1 Smooth Adaptation Law	22
3.4.2 Smooth Adaptation Simulations	24
3.4.3 Non-Smooth Adaptation Law	24
3.4.4 Non-Smooth Adaptation Simulations	25
4 Road Force Estimator	26
4.1 Individual Road Force Observer Development	26
4.1.1 Shaft Torque Observer Development	28
4.1.2 Shaft Torque Observer Simulation	29
4.2 Individual Road Force Simulation	29
4.3 Total Road Force Observer Development	30
4.4 Total Road Force Simulation	31
4.5 Combined Road Force Estimator Simulation	32

5	Experimental Testing	34
5.1	Experimental Setup	34
5.1.1	Hardware for Implementation	34
5.1.2	Hardware for Validation	36
5.2	Slip Estimation	36
5.3	Slip Based Control	39
5.4	Road Force Observation	39
5.4.1	Off-line Individual Road Force Observer	40
5.4.2	Off-line Total Road Force Observer	41
5.4.3	Off-line Combined Road Force Estimator	42
5.4.4	Real-time Combined Road Force Estimator	43
6	Conclusions	45
6.1	Slip Based Controller Summary	45
6.2	Road Force Estimator Summary	46
6.3	Future Work	47
	Bibliography	48
A	Nomenclature	50

List of Figures

1.1	PATH AHS Concept [10]	2
1.2	Highway Capacity [9]	2
1.3	Relative Vehicle Impact Velocity [10]	3
1.4	Current PATH AHS Vehicle Level Control Strategy under Braking	4
1.5	Typical Slip Curve	5
1.6	Proposed Vehicle Level Control Strategy under Braking	5
1.7	Slip Curves for Various Road Conditions	7
2.1	Vehicle and Wheel Dynamics	10
3.1	Velocity Profile and Control Effort	18
3.2	Comparison of Benchmark and Slip Based Controllers Under Nominal Conditions	19
3.3	Evaluation of Controller Robustness	20
3.4	Comparison of Benchmark and Slip Based Controllers With the Addition of Actuator Delay	21
3.5	Performance of the Benchmark Controller at Two Levels of Deceleration	22
3.6	Smooth K_B Adaptation	24
3.7	Non-Smooth K_B Adaptation	25
4.1	Shaft Torque Observer Performance with 50% Error in K	29
4.2	Individual Force Observer Performance With 50% Error in K_B and T_S	30
4.3	Total Force Observer Performance With 20% Error in M , C_d , and F_{rr}	31
4.4	Total Force Observer Performance with Noise Contaminated Velocity Measurement	32
4.5	Combined Force Estimator Performance With 50% Error in K_B and T_S	33
5.1	Stock ABS Unit	35
5.2	Torque Sensor	37
5.3	Wheel Speed and Slip Estimates	38
5.4	Slip Based and Benchmark Controller Experimental Performance	39
5.5	Slip Based and Benchmark Controller Control Effort	40
5.6	Off-line Individual Road Force Observer Performance	40
5.7	Individual Road Force Observer Weaknesses	41
5.8	Off-line Total Road Force Observer Performance	42
5.9	Off-line Combined Road Force Estimator Performance	43
5.10	Real-time Combined Road Force Estimator Performance	43

5.11 Correlation Between Real-Time Slip and Road Force Estimates	44
--	----

Abstract

Non-linear Slip-Based Brake Control and Accompanying Road Force Observation

by

Richard Charles Hill

Master of Science in Mechanical Engineering

University of California at Berkeley

Professor J. Karl Hedrick, Chair

A fundamental problem in controlling a vehicle is that the physical inputs of brake and engine torque enter into the dynamics through the wheels. This means that the desired vehicle dynamics must be related to the desired wheel dynamics in some way. Traditionally this has been done by assuming a no slip rolling condition. This report develops a new slip based controller using dynamic surface control that explicitly accounts for wheel slip. This controller is compared in simulation and physical experiment with a controller employing the limited slip assumption.

It is demonstrated that under ideal conditions the new approach offers improvement. However, the presence of uncertain measurements and actuator delay introduces chatter that significantly degrades performance. Overall it is determined that existing strategies are sufficiently robust to the limited wheel slip assumption, and for the existing level of technology the new approach is not recommended.

Related to the implementation of the slip based controller, a road force observer is also demonstrated in simulation and experiment. This observer is shown to be quite robust and accurate. Real time constraints add a time lag and noise to the estimates, but these drawbacks are relatively minor. It is ultimately proposed that this estimator be used as part of a road condition estimation scheme.

Chapter 1

Introduction

1.1 PATH AHS Concept

Freeway congestion is an increasingly serious concern for people living in and around many of the world's major metropolitan areas. The health, safety, and quality of living of people residing in these areas is adversely affected by the increasing levels of traffic. Some possible solutions to this problem include road construction, development of alternative forms of mass transit, or increasing the capacity of existing roads. Recognizing the prohibitive expense of the former two approaches, the California Partnership for Advanced Transit and Highways (PATH) has set out on a program of research in the area of Automated Highway Systems (AHS). The purpose of AHS is to improve highway throughput and safety by placing vehicles under automated control.

The basic architecture of the PATH AHS is platoons of 7 to 15 closely spaced vehicles traveling under the direction of roadside stations. This concept is illustrated in Figure 1.1. The platoons are routed using wireless communication to avoid congestion and to distribute traffic more evenly. Lane changes, and highway entry and exit are also coordinated to minimize disruption to traffic flow. At the vehicle level, on-board radar and inertial sensors are used to set speed and spacing. Vehicle lateral positioning is performed by detecting magnets embedded in the road surface. The decreased spacing between vehicles, as well as the improved traffic flow serve to greatly increase the capacity of the roadway. Figure 1.2 serves to illustrate the potential gains an AHS has to offer in increasing highway throughput.

These characteristics of an AHS also offer benefits in reducing emissions and fuel consumption. The decreased spacing helps in minimizing wind drag experienced by vehicles following the lead car in a platoon [20], while the smooth flow of traffic allows the vehicle's

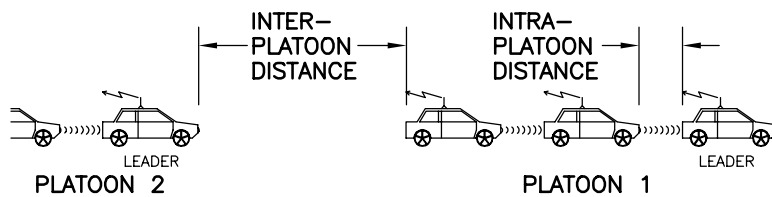


Figure 1.1: PATH AHS Concept [10]

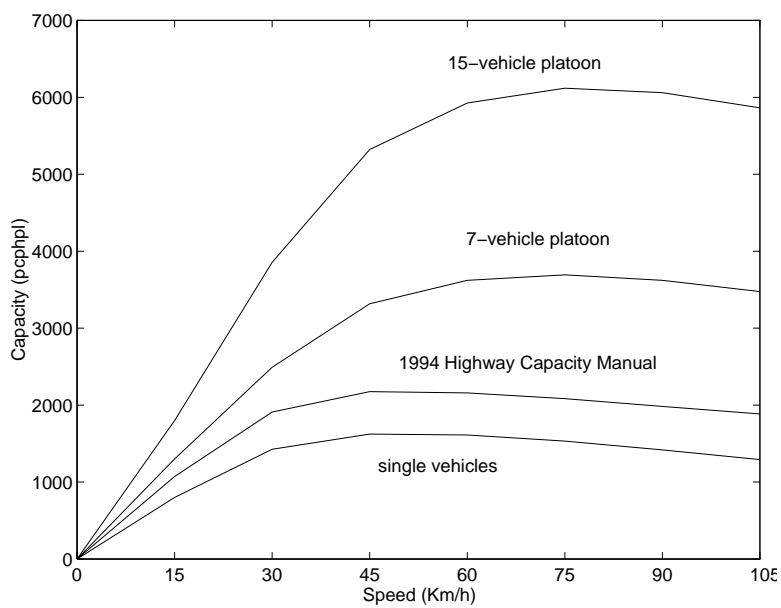


Figure 1.2: Highway Capacity [9]

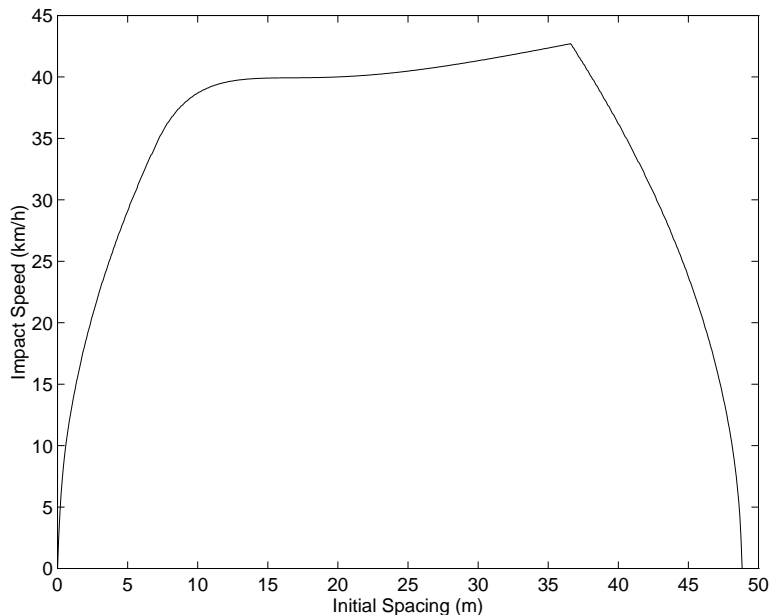


Figure 1.3: Relative Vehicle Impact Velocity [10]

engine to spend more time operating at its most efficient level.

Automated control also serves to improve the safety of highway travel. With 90% of accidents attributable to human error [3], the potential gains of automated control are substantial. Furthermore, since the AHS concept is based on close intra-platoon spacing, and distant inter-platoon spacing, the relative vehicle impact velocity in a collision is reduced [10], thereby reducing the severity of accidents. Figure 1.3 shows how the relative impact velocity varies as a function of initial spacing.

1.2 PATH AHS Program Status

Great strides have been made in the development and implementation of vehicle level control under predominantly normal operating conditions. Coordination of platoons of vehicles has also been demonstrated with the maneuvers being largely pre-programmed. More recently, PATH AHS research has moved towards demonstration of more autonomous AHS operation, as well as AHS operation under adverse or emergency conditions. Examples of this movement include work in the areas of fault detection/management, road condition estimation, and emergency braking. The work of this paper falls under the latter two categories. The support of the PATH organization under MOU 388 has enabled this work to be carried out.

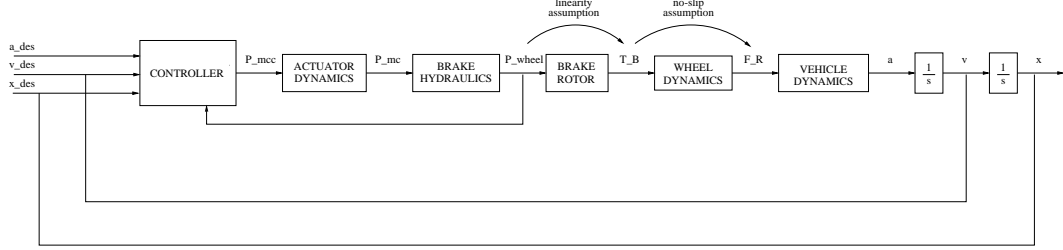


Figure 1.4: Current PATH AHS Vehicle Level Control Strategy under Braking

1.3 Motivation and Goals

Automobiles are a well suited application of non-linear control because their dynamics are highly non-linear and are often dependent on parameters that are unknown or vary over time. A standard approach for controlling non-linear systems is to linearize them and then apply standard linear control techniques. Jacobian linearization does not work well with automobiles because they have a wide range of operating points. Feedback linearization techniques on the other hand can operate over a wide range of conditions, but require a very accurate model. The necessary vehicle model would be far too complex to be practical for control purposes.

These characteristics of vehicle control are widely recognized. Under the California PATH program, AHS research has employed sliding mode control strategies to vehicle automation. Sliding mode control can essentially be thought of as a robust feedback linearizing control law. These strategies have proven effective in addressing the non-linearities and parametric uncertainties associated with vehicle control. Specifically, the PATH vehicle level control strategy has two surfaces. The outer loop controls the vehicle dynamics based on vehicle spacing error, while the inner loop controls either the brake dynamics or the intake manifold dynamics, depending on whether the vehicle is accelerating or decelerating. This strategy has been proven to work very well under normal driving conditions. Figure 1.4 illustrates the concept of the current brake control strategy.

The problem with this approach, and vehicle control in general, is that the control inputs of engine and brake torque enter in at the wheel, while it is ultimately desired to control the motion of the vehicle as a whole. In order to relate the desired vehicle dynamics to desired wheel dynamics, a limited slip assumption is applied. This is based on the familiar kinematic relationship between linear and angular velocity under rolling without slip:

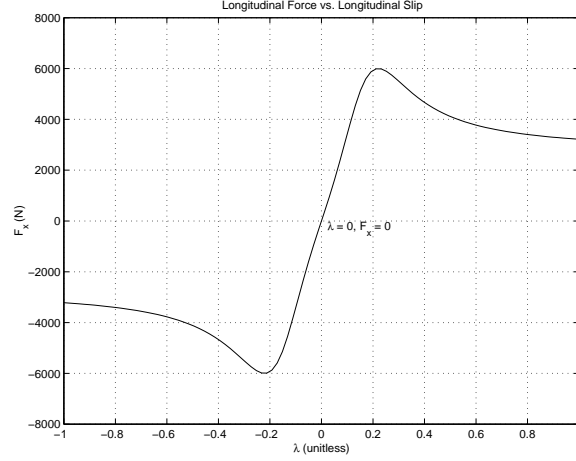


Figure 1.5: Typical Slip Curve

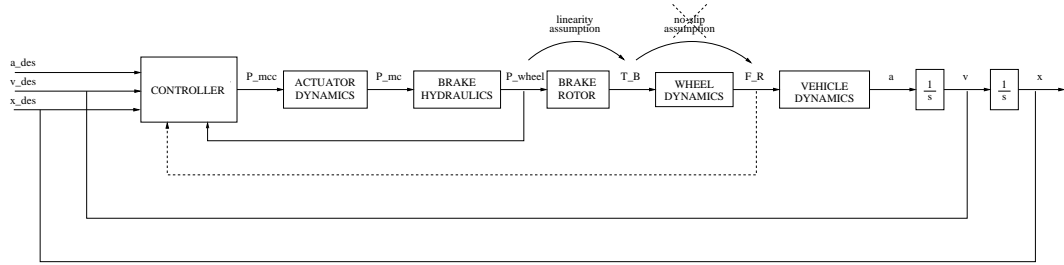


Figure 1.6: Proposed Vehicle Level Control Strategy under Braking

$$V = r\omega \quad (1.1)$$

While under normal driving this assumption is reasonable, it doesn't really hold under hard braking or acceleration. In order to overcome this limitation, this paper develops and evaluates a brake controller that uses the empirical relationship between road force and wheel slip to relate the wheel dynamics to the vehicle dynamics. Figure 1.5 shows an example of the relationship between road force and wheel slip. In addition to eliminating the no-slip assumption, the proposed controller also has an extra surface based on the error between the actual and desired road force. The concept of the proposed control strategy is shown in figure 1.6.

It has been theorized that a controller that accounts for wheel slip may be of benefit in an emergency situation, where high levels of slip are experienced. Traditionally, the control strategy in an emergency situation has been to bring a vehicle to a stop as

quickly as possible. This is the motivation behind such concepts as anti-lock brake systems (ABS). In an automated highway environment where you have vehicles traveling in platoons, stopping a vehicle as quickly as possible might result in a collision with a following vehicle. It is therefore desirable to follow a motion profile even under high slip conditions. In this situation a higher bandwidth controller may be of benefit.

As will be shown, implementation of this controller requires knowledge of the force being generated at the road tire interface, as well as knowledge of the condition of the road being traveled upon. With this in mind, this paper also develops a road force observer and an adaptive control law.

In general, road force is a difficult quantity to measure directly. It is possible to instrument the tire [2], but this is difficult and expensive. It is therefore desired to determine road force from information we already have access to. The road force estimator developed here, combines information from two individual Luenberger observers. One observer estimates each road force individually, based on the behavior of the wheel that the corresponding force is acting at. The other observer estimates the sum of the individual road forces, based on the dynamics of the vehicle as a whole. Combining the results of these two observers helps to make the overall estimator more robust to uncertainties in brake and shaft torque.

Robustness to uncertainties in brake torque also motivated the derivation of the adaptive control law presented in this paper. This adaptive algorithm estimates the brake torque gain parameter, K_B , in order to improve knowledge of brake torque magnitude.

The information on road condition is necessary for characterizing the force/slip relationship that the slip based controller is based on. Specifically, the control law presented in this paper requires knowledge of the partial derivative of road force with respect to slip, $\frac{\partial f}{\partial s}$. This quantity could be arrived at numerically, using slip measurements and road force estimates. However, since this would essentially require taking the ratio of the time derivatives of two very noisy signals, there would be a lot of error. It was determined that a better approach could be taken if knowledge of the slip curve of the road being traveled on was available. Figure 1.7 shows some typical slip curves for different road conditions. These curves are analogous to the one shown in figure 1.5, except here, the road force has been normalized by the load acting on the wheel, and only the accelerating half of the curves are shown. From this knowledge, $\frac{\partial f}{\partial s}$ could be looked up in a table indexed on the current level of slip, or road force.

Due to the relevance of road condition on vehicle performance and control, there has been a significant amount of research performed in the area of its determination. One

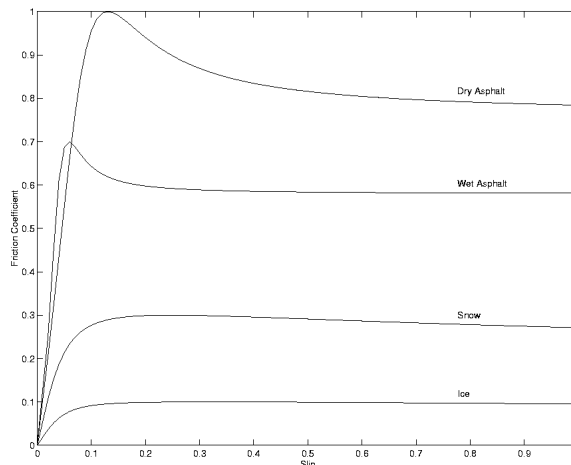


Figure 1.7: Slip Curves for Various Road Conditions

approach has been to employ optical sensors [6] [18]. This method basically inundates a patch of road with light, and identifies its condition based on the intensity and spectrum of the reflected light.

Some other methodologies attempt to identify road condition without the use of any specialized sensors. The primary basis for these methodologies is experimental work that demonstrates road condition can be characterized by the relationship of normalized road force and tire slip. This concept is illustrated in figure 1.7. The road force observer mentioned previously could be applied to this type of approach. It is left for future work to actually classify the road condition based on the slip and road force information acquired in this work.

An approach that falls into this category estimates road condition based on the slope of the slip curve near origin [5]. Other approaches try and match parameters of various tire models through least squares estimation [11], Bayesian selection [15], and neural networks [13].

A lot of the work done in the area of road condition estimation lacks experimental validation. Those that do primarily demonstrate performance by identifying various road surfaces. Little emphasis is placed on the intermediate step of estimating and validating the road force itself. The work of this paper attempts to address this deficiency.

Furthermore, the controller proposed above will be assessed throughout the course of this paper. Its performance will be evaluated in regards to sampling time, parametric uncertainties, and actuator delay. Feasibility of the controller will be determined with respect to a controller that does employ a limited slip assumption. Ultimately a determination will be made as to whether or not wheel slip seriously degrades the current controller's performance.

Chapter 2

Control Model

In our system there are two levels of dynamics that we are concerned with. One level is the dynamics of the vehicle as a whole, and the other is associated with the dynamics of the wheels. We ultimately want to control the vehicle, but have to do so through our control inputs that enter in at the wheels. Figure 2.1 illustrates the model that will be employed in our controller.

2.1 Vehicle Dynamics

The forces we are concerned with that influence vehicle motion are the sum of the road forces acting at each wheel (F), and the losses due to wind drag ($C_d V^2$) and rolling resistance (F_{rr}). The equation of motion of the vehicle can be seen in equation 2.1.

$$\dot{V} = \frac{1}{M}(F - C_d V^2 - F_{rr}) \quad (2.1)$$

This model only takes into account longitudinal forces. It is assumed that under highway travel, the roads will have only gentle curves, so longitudinal forces will dominate.

2.2 Wheel Dynamics

The motion of each individual wheel is determined by the torque of the road (rf), the brake torque (T_B), and the shaft torque (T_S) from the drive shaft. The shaft torque is approximated as being split evenly between the two drive wheels. This is reasonable for straight line motion on a road where each wheel is on the same type of surface. The rolling resistance doesn't contribute a moment because it is modeled as causing a shift in

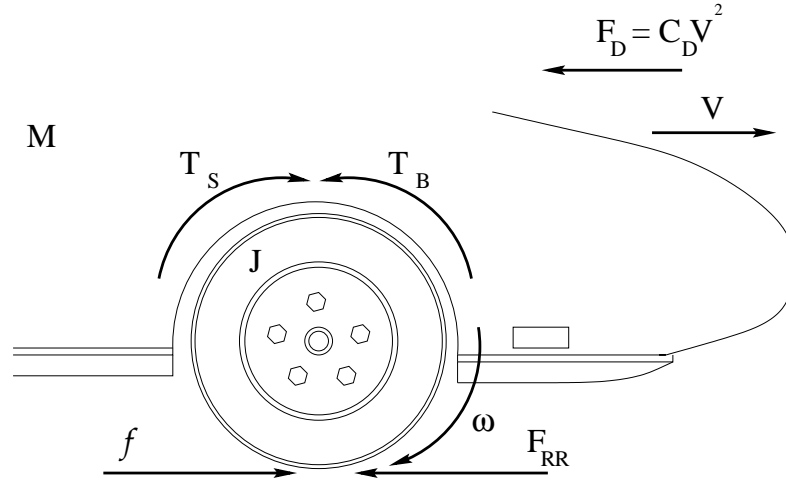


Figure 2.1: Vehicle and Wheel Dynamics

the location of the normal force acting on the wheel, such that the moment of the rolling resistance is offset. Equation 2.2 illustrates the equation of motion of the i_{th} wheel.

$$\dot{\omega}_i = \frac{1}{J_i} \left(\frac{T_S}{2} - r_i f_i - T_{Bi} \right) \quad (2.2)$$

2.2.1 Brake Torque

For control, brake torque is modeled as being linearly proportional to brake pressure at the wheel, P_w . Neglecting 'pushout' pressure, and assuming operation under low levels of slip, this model is reasonably accurate.

$$T_{Bi} = \alpha_i K_B P_w \quad (2.3)$$

Over time and under different braking conditions however, the quantity K_B can vary as much as 50% under normal driving conditions. The linearity of this relationship especially breaks down under high-slip conditions, which we are particularly concerned with in this application. Here the constant K_B represents the relationship between brake pressure and brake torque for the vehicle as a whole. The constant α_i represents the percentage of the total brake torque that is distributed to each wheel. The brake pressure at each wheel is identical in steady state.

2.2.2 Shaft Torque

Shaft torque is modeled as being generated from the drive axle shaft, where the shaft is treated as a torsional spring.

$$\dot{T}_S = K(R_d\omega_{cr} - \omega_w) \quad (2.4)$$

K is the spring constant for the shaft, R_d is the final drive ratio, ω_{cr} is the transmission carrier speed, and ω_w is the average of the two rear wheel speeds. The differential equation for transmission carrier speed is as follows:

$$\dot{\omega}_{cr} = \frac{1}{J_{cr,i}} \left(\frac{T_t}{R_i} - R_d T_S \right) \quad (2.5)$$

$J_{cr,i}$ is the carrier inertia associated with the i -th gear ratio, T_t is the torque from the turbine side of the torque converter, and R_i is the i -th gear ratio.

2.3 Tire Model

For the formulation of this problem, it will be assumed that we have knowledge of the empirical relationship between slip and road force. In particular, the Bakker-Pacejka 'Magic Tyre Formula' of the form shown in equation 2.6 is employed [1]. Since this is a very complex function, the quantity $\frac{\partial f}{\partial s}$ is determined by means of a look up table. It could also be calculated numerically, but this may add more noise. This all presumes that in implementation, there will be a limited set of slip curves associated with different road conditions that can be chosen from. It is therefore necessary that the controller be robust to errors in the tire model. Here it is again assumed that the vehicle is experiencing purely longitudinal motion.

$$\mu = D \sin (C \arctan [B(s + S_h) - E(B(s + S_h) - \arctan(B(s + S_h)))]]) \quad (2.6)$$

The quantity of longitudinal slip, s , is calculated from equation 2.7. Slip is essentially the normalized difference between the vehicle's actual longitudinal velocity and what the velocity would be under pure rolling. Here longitudinal slip is negative under braking and positive under acceleration. The wheel speed (ω) is readily available from sensors that come standard on most all modern cars. The acquisition of the vehicle's translational velocity (V) however is much harder to come by. This is due to the fact that under braking, all wheels experience significant amounts slip, and therefore V cannot be found from the

no-slip rolling condition. For our purposes, we will assume we have access to V . In implementation, some sort of observer would have to be employed. All in all, slip is a difficult quantity to measure, so our controller must be robust to errors in it as well.

$$s = \frac{r\omega - V}{\max(r\omega, V)} \quad (2.7)$$

The quantity μ in equation 2.6 represents the longitudinal road force experienced at a wheel, normalized by the load acting on it. It is essentially the coefficient of friction associated with the road/tire interface.

$$\mu = \frac{f_i}{f_{N,i}} \quad (2.8)$$

A typical relationship between slip and road force was illustrated in figure 1.5

Chapter 3

Slip Based Dynamic Surface Controller

3.1 State Equations

Ultimately it is the goal for the proposed controller to achieve tracking of some desired velocity profile. The derivative of the vehicle linear velocity is expressed in equation 2.1. Our physical input under braking is master cylinder pressure, which does not appear explicitly in this equation.

Taking the derivative of the road force at each wheel makes the wheel dynamics appear through the empirical relationship between road force and wheel slip.

$$\dot{F} = \Sigma \frac{\partial f_i}{\partial s_i} \dot{s}_i = \Sigma \frac{\partial f_i}{\partial s_i} \left(\frac{r_i \omega_i}{V} - \frac{r_i \omega_i \dot{V}}{V^2} \right) \quad (3.1)$$

Substituting in the wheel dynamics from equation 2.2 and the vehicle dynamics from equation 2.1, one can see that our control input, master cylinder pressure, now has access to our states through the brake pressure at the wheel. This can be seen in equation 3.2.

$$\dot{F} = \Sigma \frac{\partial f_i}{\partial s_i} \left(\frac{r_i}{J_i V} \left(\frac{T_S}{2} - r_i f_i - \alpha_i K_B P_w \right) - \frac{r_i \omega_i}{M V^2} (F - C_d V^2 - F_{rr}) \right) \quad (3.2)$$

The brake pressure at the wheel enters into the physical dynamics of the system through the quantity of brake torque. The relationship in equation 2.3 is utilized. Here it is assumed that P_w will be the same at each wheel in steady state.

One can see the non-linearities inherent in these equations. Furthermore, there are uncertainties of some degree associated with most all of the parameters, including in

equation 2.1, where the control input does not appear explicitly. The non-linearity and mismatched uncertainty of the state equations make this system well suited for a dynamic surface controller. This is the approach taken here.

3.2 Controllability

Before we go into the controller design, we will perform an examination of the controllability of our system. Since this is a non-linear system, the only conclusions we can draw about controllability are local. A test for local controllability (accessibility), comes from a rank test of \overline{C} . \overline{C} is defined below for a two state system, where $[f,g]$ is a Lie Bracket:

$$\overline{C} = [g(x), [f(x), g(x)]] \quad (3.3)$$

If \overline{C} is full rank, then our system is accessible. Even though our system essentially has five states, we will treat the sum of the individual road forces as a single state, since the same P_w is applied to all the wheels. The state equations for our system are hence defined by equations 2.1 and 3.2. In order to examine accessibility, we need to put our system into an affine form:

$$\dot{\mathbf{x}} = \overbrace{\begin{bmatrix} \frac{1}{M}(F - C_d V^2 - F_{rr}) \\ \sum \frac{\partial f_i}{\partial s_i} \left(\frac{r_i}{J_i V} \left(\frac{T_S}{2} \right) - \frac{r_i \omega_i}{M V^2} (F - C_d V^2 - F_{rr}) \right) - \beta F \end{bmatrix}}^{f(\mathbf{x})} + \overbrace{\begin{bmatrix} 0 \\ -\sum \frac{\partial f_i}{\partial s_i} \frac{r_i \alpha_i K_B}{J_i V} \end{bmatrix}}^{g(\mathbf{x})} P_w$$

In order to perform the partial derivatives required by the Lie Bracket, the following substitution was made:

$$\sum \frac{\partial f_i}{\partial s_i} \frac{r_i^2 f_i}{J_i V} = \beta F \quad (3.4)$$

The resultant \overline{C} is as follows:

$$\begin{bmatrix} 0 & -\sum \frac{\partial f_i}{\partial s_i} \frac{r_i \alpha_i K_B}{M J_i V} \\ \sum \frac{\partial f_i}{\partial s_i} \frac{r_i \alpha_i K_B}{M J_i V} & * \end{bmatrix} \quad (3.5)$$

From observation, one can see that the determinant of this matrix is nonzero, and hence the matrix is full rank. Therefore our system is indeed accessible, and we can proceed with the controller design with some confidence that our system can be controlled.

3.3 Dynamic Surface Controller

The idea behind the design of this controller is that we can use the empirical relationship between road force and slip to avoid reliance on a no-slip rolling condition. This is the approach taken in [8], where a non-linear controller was designed to account for coupling of lateral and longitudinal dynamics.

3.3.1 Controller Design

As was mentioned before, a dynamic surface sliding mode approach was taken in the design of this controller. Presuming that our vehicle is traveling in a platoon of several vehicles, it is ultimately our goal to track some desired velocity profile while maintaining a desired level of spacing with the vehicle we are following. A sliding surface, s_1 , is defined in terms of our spacing error, ε . It is desired to choose s_1 and our control input such that the derivative of a candidate Lyapunov function of the form $V = \frac{1}{2}s_1^2$ is negative definite. If this is done, we are guaranteed that s_1 is asymptotically stable, thereby indicating that our error ε goes to zero in finite time.

We will define our surface such that once s_1 reaches its sliding phase, where it is on average equal to zero, our error ε will go to zero exponentially.

$$s_1 = \dot{\varepsilon} + \lambda\varepsilon = 0 \quad (3.6)$$

Choosing our control input such that the equation 3.7 is satisfied will guarantee that our candidate Lyapunov function is negative definite. The size of η_1 determines the speed with which our controller reaches the sliding phase.

$$\dot{s}_1 = -\eta_1 s_1 \quad (3.7)$$

Taking the derivative of our surface s_1 :

$$\dot{s}_1 = \ddot{\varepsilon} + \lambda\dot{\varepsilon} = (a - a_{des}) + \lambda\dot{\varepsilon} = -\eta_1 s_1 \quad (3.8)$$

We can then plug in for a using equation 2.1.

$$\dot{s}_1 = \frac{1}{M}(F - C_d V^2 - F_{rr}) - \Delta_V - a_{des} + \lambda\dot{\varepsilon} = -\eta_1 s_1 \quad (3.9)$$

Normally one would then use the control input to overpower the uncertainty in our control model (Δ_V) to guarantee that the derivative of our candidate Lyapunov function is negative definite:

$$\dot{V} = s_1(-\eta_1 s_1 + \Delta_V) \quad (3.10)$$

Since our control input, P_w , does not appear explicitly in our equation, we will treat F_{des} as a sort of a “synthetic” input.

$$F_{des} = \overbrace{[-\eta_1 s_1 - |\Delta_V|_{\max} s_1 - \lambda \dot{e} + a_{des}]}^{-K_1 s_1} M + C_d V^2 + F_{rr} \quad (3.11)$$

K_1 can then be chosen analytically if the bounds on Δ_V are known. In this case, Δ_V includes all parametric uncertainties as well as the unmodelled dynamics. Since an analytical bound can't really be arrived at, the gain K_1 (as well as λ) were basically just tuned until a desirable level of performance was achieved.

Now that we have determined an F_{des} that achieves our control goal, we need to guarantee that F actually converges to F_{des} . Following the same design procedure as above, we define a second surface.

$$s_2 = F - F_{des} = 0 \quad (3.12)$$

$$\dot{s}_2 = \dot{F} - \dot{F}_{des} = -\eta_2 s_2 \quad (3.13)$$

Substituting for \dot{F} from equation 3.2:

$$\dot{s}_2 = \Sigma \frac{\partial f_i}{\partial s_i} \left(\frac{r_i}{J_i V} \left(\frac{T_S}{2} - r_i f_i - \alpha_i K_B P_w \right) - \frac{r_i \omega_i}{M V^2} (F - C_d V^2 - F_{rr} - M \Delta_V) \right) - \Delta_F - \dot{F}_{des} = -\eta_2 s_2 \quad (3.14)$$

Now our physical control input P_w appears in our equations. Solving for P_w gives us our control law, where we again use the input to overpower our uncertainty.

$$P_{w,des} = [-\Sigma \frac{\partial f_i}{\partial s_i} \frac{r_i}{J_i V} \alpha_i K_B]^{-1} [\Sigma \frac{\partial f_i}{\partial s_i} \frac{r_i}{J_i V} (r_i f_i - \frac{T_S}{2}) + \Sigma \frac{\partial f_i}{\partial s_i} \frac{r_i \omega_i}{M V^2} (F - C_d V^2 - F_{rr}) - \underbrace{\Sigma \frac{\partial f_i}{\partial s_i} \frac{r_i \omega_i}{V^2} |\Delta_V|_{\max} s_2 - |\Delta_F|_{\max} s_2 - \eta_2 s_2 + \dot{F}_{des}}_{-K_2 s_2}] \quad (3.15)$$

The quantity \dot{F}_{des} requires taking the derivative of an uncertainty. This is highly undesirable. Instead, we will approximate \dot{F}_{des} by a filtered state. This step is what differentiates dynamic surface control from other similar methods. Notice that our control law divides through by $\frac{\partial f_i}{\partial s_i}$. This is of concern since $\frac{\partial f_i}{\partial s_i}$ goes to zero around the peak of the slip curve. The controller derivation in [8] addresses this by defining the second surface in

terms of slip error rather than force error. We chose not to take this approach since slip is a quantity that is different at each individual wheel. With our second surface being based on the sum of the individual road forces, this problem is overcome. In implementation, the problem of division by zero is handled in an adhoc manner.

$$\dot{F}_{des} \approx \dot{F}_{des, filt} = \frac{F_{des} - F_{des, filt}}{\tau} \quad (3.16)$$

By choosing τ sufficiently small, the lag due to the filter will be minimal, and the approximation will be quite good. This approach is more theoretically sound than mere numerical differentiation. The gain associated with this surface, K_2 , was also determined by tuning it until a desired level of performance was achieved.

3.3.2 Benchmark Controller

The purpose of designing this controller was to achieve improved performance over existing control strategies that use a limited slip assumption in their derivation. This section of the paper compares the performance of our controller against a variation that employs a limited slip assumption. The comparisons here are based on simulations performed in the *comb_sim* simulation package. This is a fairly comprehensive package written in C, that employs a 33 state vehicle model for evaluation. Despite the complexity of the vehicle model employed in the simulation, these results should only be considered for qualitative analysis.

For the purpose of comparison, our benchmark controller will employ the same upper level surface as is used in the above proposed controller. This surface results in the formulation of F_{des} derived in equation 3.11. This surface is analogous to the one used in the existing PATH control strategy [16], except for the fact that that surface utilizes lead car information to ensure that errors do not propagate as they are passed down the length of a platoon. For the sake of simplicity, we chose not to use this surface.

Instead of employing the same second surface as is used in our proposed controller, the benchmark controller will employ a no slip rolling condition to algebraically relate F_{des} to our control input, $P_{w, des}$. Specifically, the individual wheel equations represented by equation 2.2 are summed to arrive at the following:

$$J(\Sigma \dot{\omega}_i) = T_S - T_B - rF \quad (3.17)$$

Assuming no slip rolling we have:

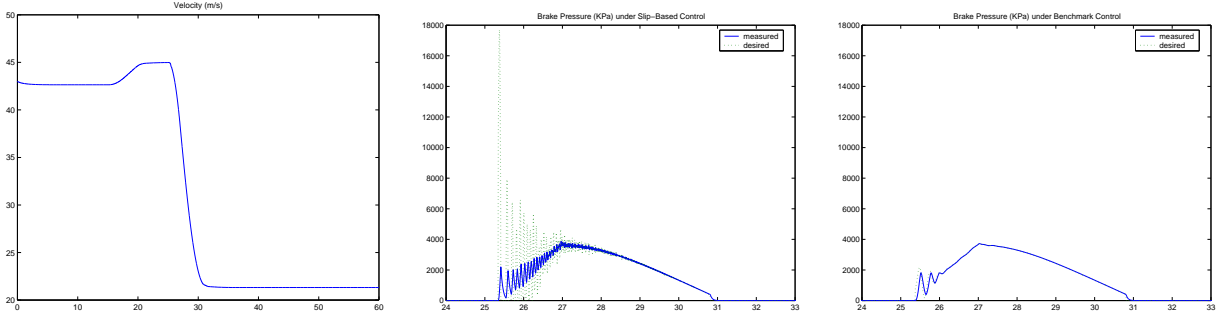


Figure 3.1: Velocity Profile and Control Effort

$$\dot{\omega}_{lf} = \dot{\omega}_{rf} = \dot{\omega}_{rr} = \dot{\omega}_{lr} = \frac{\dot{V}}{r} \quad (3.18)$$

Using equation 2.1 and 2.3, we can substitute for \dot{V} and T_B respectively in the above two equations. Combining equations 3.17 and 3.18 then leaves us with the following:

$$\frac{4J}{rM}(F - C_dV^2 - F_{rr}) = T_S - K_B P_w - rF \quad (3.19)$$

Rearranging the above gives us our benchmark control law:

$$P_{w,des} = \frac{1}{K_B} \left[T_S - \frac{4J}{rM}(F_{des} - C_dV^2 - F_{rr}) - rF_{des} \right] \quad (3.20)$$

Again for the sake of simplicity, the final brake surface was omitted. This surface determines the desired master cylinder pressure based on $P_{w,des}$ [9]. Its purpose is to account for the dynamics of the hydraulic brake system.

3.3.3 Nominal Simulations

The velocity profile used for testing these two controllers in simulation was a simple trapezoidal profile. The braking portion of the profile, which is of interest to us, consisted of an event that ramps up to and down from a maximum deceleration of $8 \frac{m}{s^2}$. This profile can be seen in figure 3.1.

For this profile, the two controllers were first run in simulation under completely ideal conditions. Control effort was applied in intervals of 6 msec, and each controller had complete knowledge of all parameters and sensor measurements. The velocity and spacing error for the braking portion of this maneuver are shown in figure 3.2. From examination of this figure, one can see that the slip based controller offers an improvement in both spacing and velocity error over the benchmark controller. It is interesting to note that in the case of both controllers, velocity and spacing errors reach a maximum at the onset and halt of the

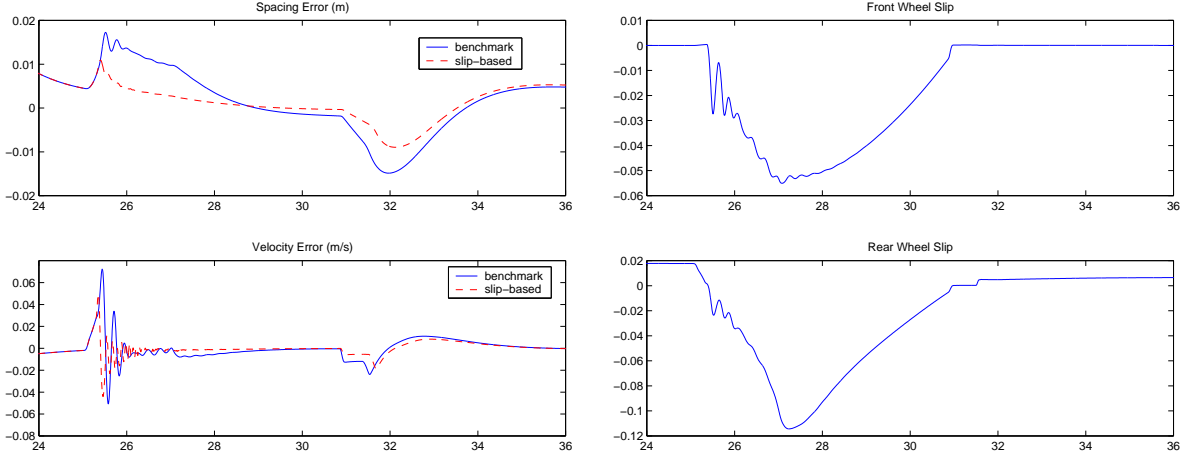


Figure 3.2: Comparison of Benchmark and Slip Based Controllers Under Nominal Conditions

braking event. Figure 3.2 also shows the level of slip experienced at a front and rear wheel under this maneuver. The level of slip experienced under both controllers is essentially the same.

Figure 3.1 also shows the control effort desired and achieved at the wheel for each controller. One can observe that the control effort for the slip based controller is more oscillatory than the benchmark controller. This chatter can be reduced by decreasing the gain associated with the second surface, this however degrades controller performance. Notice in each case that the control signal is not always chattering. The formulation of this controller results in an implied boundary layer that the error surfaces remain within, it is therefore not necessary that either controller chatter around its desired trajectory.

3.3.4 Robustness Simulations

Since the operation of these controllers depend on the availability of some information that is rather difficult to obtain, it is important that the controllers be robust to uncertainties. In particular, the measurement of the quantities of slip, road force, and velocity, are difficult to sense. Furthermore, the parameter K_B is known to change significantly under operation, especially at high-levels of slip.

In order to evaluate robustness, simulations were run with error imposed on various sensor measurements and parameter values. The graphs on the lefthand side of figure 3.3 are from one such run. In this simulation, the vehicle mass is in error by 25%, coefficient of drag and rolling resistance are in error by 10%, and K_B is in error by 50%. Furthermore, the interval at which control effort is applied has been increased to 18 msec. Examination of

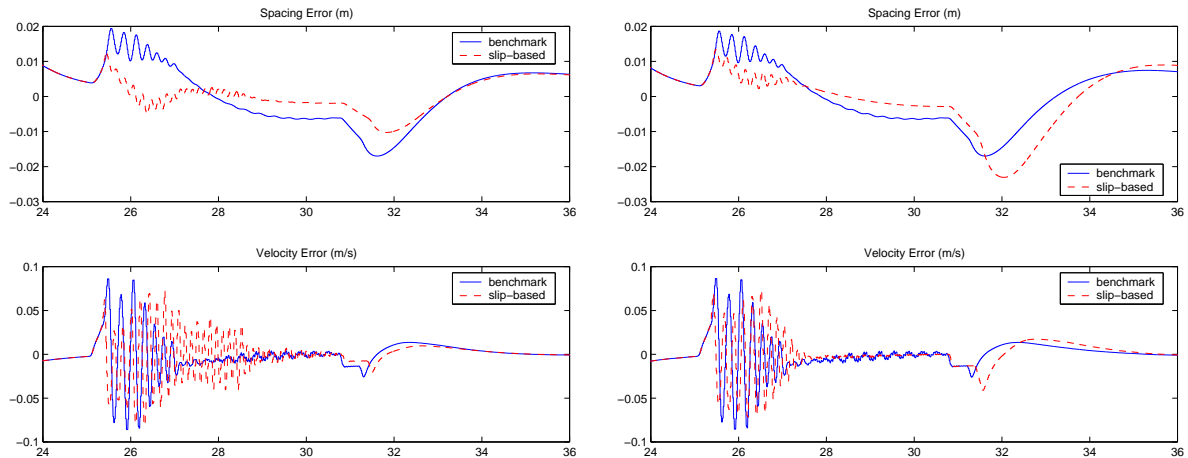


Figure 3.3: Evaluation of Controller Robustness

these graphs shows that both controllers are quite robust to the uncertainty and increased sampling time. Under these conditions the slip-based controller still offers an improvement over the benchmark controller. Examination of the error profiles seems to indicate that this improvement in performance is due to the extra surface, not the fact that the new formulation takes into account wheel slip. The maximum level of wheel slip is reached somewhere in the neighborhood of 27 sec, and does not necessarily seem to correspond an increase in the velocity or spacing error.

Another set of simulations run to further assess robustness are shown in the right half side of figure 3.3. In order to degrade the slip “measurement” in these simulations, the wheel speed signal used in the calculation is contaminated by white noise. Furthermore, the controller used a measure of slip slope that was in error by 10%. Notice the importance of the value of $\frac{\partial f}{\partial s}$ in the slip based control law. Since the slip measurements and tire model are necessary for the operation of the slip based controller, error in these two areas degraded performance. Though the slip based controller proved to be quite robust, this added uncertainty degraded performance enough that the benchmark controller ultimately had smaller spacing and velocity error than the slip based controller.

Another factor that needs to be considered in the operation of these controllers is actuator dynamics. Since a brake actuator needs to generate a sizeable amount of force, it is likely that the actuator will be hydraulic in nature. This type of actuator will have some sort of delay associated with it. In order to assess the effect of actuator dynamics, simulations were run that included a 42 msec pure time delay and a 50 msec first order lag on the commanded master cylinder pressure. The results of these simulations are shown in figure 3.4. Here one can see that the performance of the two controllers under these

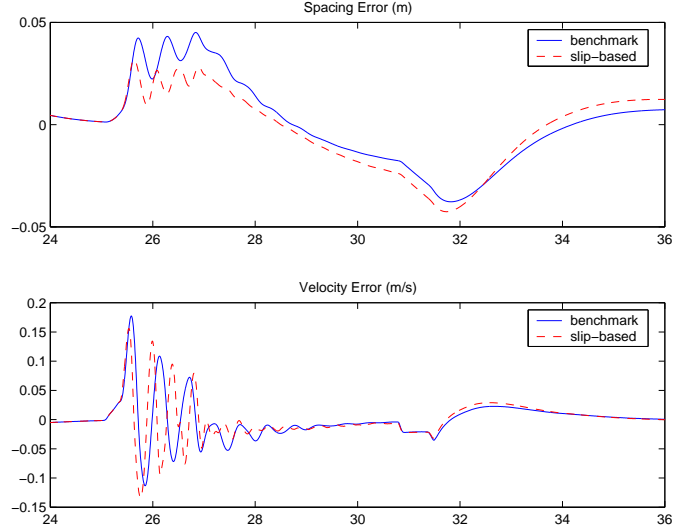


Figure 3.4: Comparison of Benchmark and Slip Based Controllers With the Addition of Actuator Delay

conditions is comparable.

Simulation under nominal conditions demonstrated that the slip-based controller offered improved performance over the benchmark controller. It was also shown that the gain on the second surface that provided this improvement resulted in increased chatter. The addition of measurement uncertainty and actuator delay increased the level of chattering to the point that the gain on the second surface had to be decreased. This lower level gain did not provide improved performance over the benchmark controller. In simulation, additional factors that affected chattering were the time constant associated with $F_{des, filt}$, as well as the characteristic slip curve of the road being traveled upon. These results give some indication that the increased level of chatter of the slip based controller is related to the added filter dynamics and added slip dynamics associated with the second surface.

3.3.5 Contribution of the Limited Slip Assumption

The simulations of the previous two sections raise the question, how much does the limited slip assumption really affect controller performance. Examination of the preceding error profiles seem to indicate that there isn't much of a correspondence between high levels of slip and high levels of tracking error. To further investigate, the simulations shown in figure 3.5 were run. Here the benchmark controller was run at two levels of deceleration, 8 and $3\frac{m}{s^2}$, where the larger deceleration corresponds to a larger level of slip. Examination of these graphs seems to indicate that the limited slip assumption is not that detrimental to controller performance.

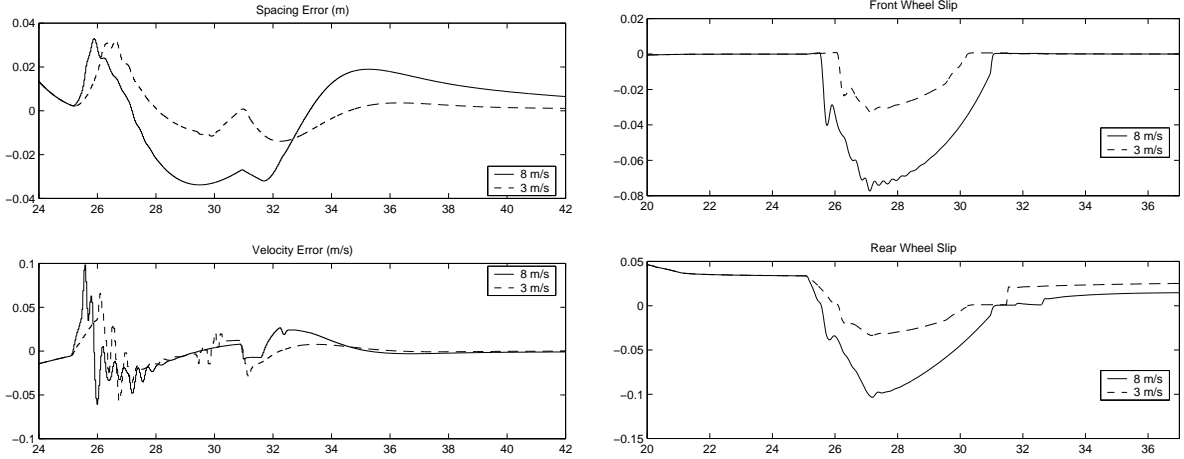


Figure 3.5: Performance of the Benchmark Controller at Two Levels of Deceleration

3.4 Adaptive Dynamic Surface Controller

Though each of these controllers were shown to be quite robust to parameter uncertainty, in the case of the slip based controller, it is still necessary that the characteristic slip curve of the road being traveled on be identified. It will be shown that this determination relies heavily on accurate knowledge of the brake torque parameter K_B . Recognizing this, we set out in this section of the paper to derive a controller that adapts K_B for this purpose. [9] also derives an adaptive control law for estimating K_B . This control law relies on the no slip rolling condition we are trying to avoid.

3.4.1 Smooth Adaptation Law

The design of the adaptive dynamic surface controller builds off what was done earlier. The idea is that we extend our state by the parameter estimate error, then define a new candidate Lyapunov function as follows:

$$V = \frac{1}{2}s_1^2 + \frac{1}{2}s_2^2 + \frac{\gamma}{2}\tilde{K}_B^2 \quad (3.21)$$

Again it is desired that our parameter estimation law be chosen to ensure that \dot{V} is at least negative semi-definite.

$$\dot{V} = s_1\dot{s}_1 + s_2\dot{s}_2 + \gamma\tilde{K}_B\dot{\tilde{K}}_B \quad (3.22)$$

If we make the assumption that K_B varies slowly, then we have that $\dot{\tilde{K}}_B \approx -\dot{K}_B$. Plugging in for $\dot{\tilde{K}}_B$, \dot{s}_1 , and \dot{s}_2 from equation 3.14, we get the following:

$$\dot{V} = -K_1 s_1^2 + s_2 \left[-\Gamma + \frac{K_B}{\hat{K}_B} (\Gamma - K_2 s_2) \right] - \gamma \tilde{K}_B \dot{\hat{K}}_B \quad (3.23)$$

where:

$$\Gamma = \Sigma \frac{\partial f_i}{\partial s_i} \frac{r_i}{J_i V} \left(\frac{T_S}{2} - r_i f_i \right) + \Sigma \frac{\partial f_i}{\partial s_i} \frac{r_i \omega_i}{M V^2} (F - C_d V^2 - F_{rr}) + \dot{F}_{des, filt} \quad (3.24)$$

Note that we have substituted our control law into the expression for \dot{s}_2 . Our control law is formulated using our estimate of the brake torque gain \hat{K}_B , and our uncertainties are bounded. We have also used the filtered approximation of \dot{F}_{des} again. Using the identity $\frac{K_B}{\hat{K}_B} = \frac{\tilde{K}_B}{\hat{K}_B} + 1$ we get the following:

$$\dot{V} = -K_1 s_1^2 - K_2 s_2^2 + \frac{\tilde{K}_B s_2}{\hat{K}_B} (\Gamma - K_2 s_2) - \gamma \tilde{K}_B \dot{\hat{K}}_B \quad (3.25)$$

Choosing our adaptation law as follows:

$$\dot{\hat{K}}_B = \frac{s_2}{\gamma \hat{K}_B} (\Gamma - K_2 s_2) \quad (3.26)$$

\dot{V} reduces to:

$$\dot{V} = -K_1 s_1^2 - K_2 s_2^2 \quad (3.27)$$

This indicates that \dot{V} is negative semidefinite. This result allows us to conclude that s_1 , s_2 , and \tilde{K}_B are bounded. Examining \ddot{V} :

$$\ddot{V} = 2K_1^2 s_1^2 + 2K_2^2 s_2^2 \quad (3.28)$$

Since we know that s_1 and s_2 are bounded, we can conclude that \ddot{V} is bounded. This implies that \dot{V} is uniformly continuous. This result combined with the fact that V is lower bounded, and \dot{V} is negative semi-definite, allows us to conclude based on Barbalat's Lemma, that $\dot{V} \rightarrow 0$. This indicates that s_1 and $s_2 \rightarrow 0$, and in turn $\dot{s}_2 \rightarrow 0$. Examining \dot{s}_2 :

$$\dot{s}_2 = \frac{\tilde{K}_B}{\hat{K}_B} (\Gamma - K_2 s_2) - K_2 s_2 \rightarrow 0 \quad (3.29)$$

Since s_2 goes to zero, and \hat{K}_B is bounded, we know that $\tilde{K}_B \Gamma \rightarrow 0$. If we get sufficient excitation such that $\Gamma \neq 0$, then our parameter estimate error $\tilde{K}_B \rightarrow 0$.

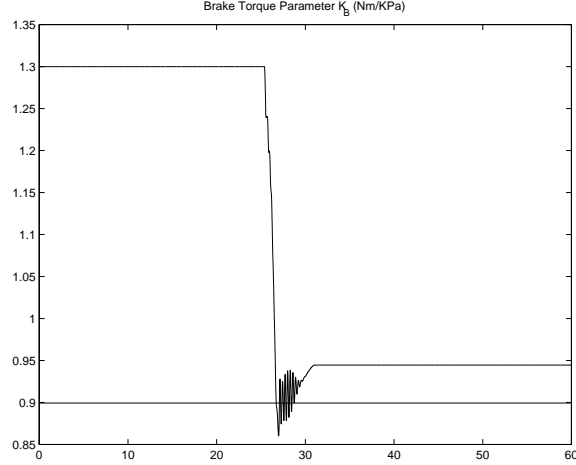


Figure 3.6: Smooth K_B Adaptation

3.4.2 Smooth Adaptation Simulations

To evaluate if our above hypothesis makes sense, some simulations were run to see if \tilde{K}_B does indeed converge to zero. Our simulation velocity profile was again a trapezoid. Figure 3.6 shows an example of one simulation run. The estimate essentially converges to the correct value. It should be noted that this simulation was run with parameter and measurement uncertainty, as well as actuator delay. The addition of these effects did not seem to have much effect on parameter estimate convergence. It is possible that if a richer velocity profile was used, better convergence could be achieved.

3.4.3 Non-Smooth Adaptation Law

We will now try a variation on the above adaptation law. The thought is that by adding a signum function to our adaptation law, the switching will increase the excitation and will improve the rate of convergence. Below is the new non-smooth adaptation law:

$$\dot{\hat{K}}_B = \frac{\text{sgn}(s_2)}{\gamma \hat{K}_B} (\Gamma - K_2 s_2) \quad (3.30)$$

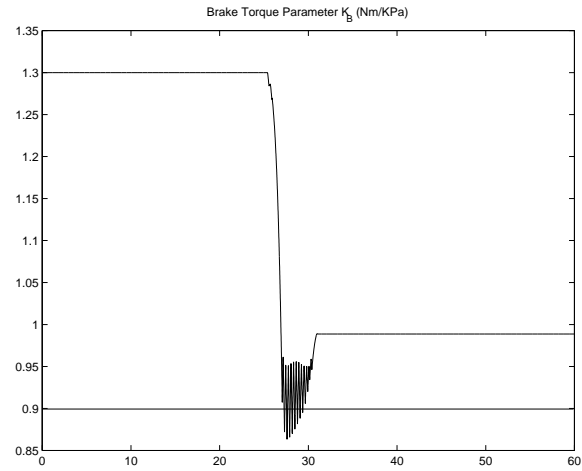


Figure 3.7: Non-Smooth K_B Adaptation

3.4.4 Non-Smooth Adaptation Simulations

Figure 3.7 shows the performance of the new adaptation law. Performance is basically comparable to the case of smooth adaptation.

Chapter 4

Road Force Estimator

For our controller development we looked at two states. One of these states was the sum of the individual road forces. For any road identification scheme, we would need to have knowledge of the magnitude of each of the forces individually. Essentially our approach for accomplishing this estimation task is to combine the results from two different observers. One observer estimates each of the individual road forces based on a dynamic wheel model. This observer is susceptible to errors in estimation of brake and shaft torque. The other observer estimates the sum of the road forces based on a dynamic vehicle model. The estimate of the sum of the road forces is then used to scale the estimates of the individual road forces. This scheme overcomes the susceptibility to errors in brake and shaft torque, as long as the distribution of brake and shaft torque is known. This approach allows us to decouple the contribution of each of the correction terms.

4.1 Individual Road Force Observer Development

This section develops the individual road force observer. The basic approach is to build models of each of the wheels, and to correct our estimate of the road force based on the wheel speed signals. In our controller development, our force state relied on $\frac{\partial f_i}{\partial s_i}$. Since we don't have any knowledge of the slip curve at this point, we will assume that our road force is constant, and will rely on our correction term to drive our force estimate in the right direction. Below are our state equations:

$$\dot{\omega}_i = \frac{1}{J_i} \left(\frac{T_S}{2} - r_i f_i - \alpha_i K_B P_w \right) \quad (4.1)$$

$$\dot{f}_i = 0 \quad (4.2)$$

Since these equations are entirely linear, we will start by designing a Luenberger Observer. Discretizing the state equations above for a sample time of t_s , we end up with the following state space formulation:

$$\begin{bmatrix} f_{fl}(k+1) \\ f_{fr}(k+1) \\ f_{rr}(k+1) \\ f_{rl}(k+1) \\ \omega_{fl}(k+1) \\ \omega_{fr}(k+1) \\ \omega_{rr}(k+1) \\ \omega_{rl}(k+1) \end{bmatrix} = \begin{bmatrix} 1 & 0 & 0 & 0 & 0 & 0 & 0 & 0 \\ 0 & 1 & 0 & 0 & 0 & 0 & 0 & 0 \\ 0 & 0 & 1 & 0 & 0 & 0 & 0 & 0 \\ 0 & 0 & 0 & 1 & 0 & 0 & 0 & 0 \\ \frac{-r_{fl}t_s}{J_{fl}} & 0 & 0 & 0 & 1 & 0 & 0 & 0 \\ 0 & \frac{-r_{fr}t_s}{J_{fr}} & 0 & 0 & 0 & 1 & 0 & 0 \\ 0 & 0 & \frac{-r_{rr}t_s}{J_{rr}} & 0 & 0 & 0 & 1 & 0 \\ 0 & 0 & 0 & \frac{-r_{rl}t_s}{J_{rl}} & 0 & 0 & 0 & 1 \end{bmatrix} \begin{bmatrix} f_{fl}(k) \\ f_{fr}(k) \\ f_{rr}(k) \\ f_{rl}(k) \\ \omega_{fl}(k) \\ \omega_{fr}(k) \\ \omega_{rr}(k) \\ \omega_{rl}(k) \end{bmatrix} + \begin{bmatrix} 0 & 0 & 0 & 0 \\ 0 & 0 & 0 & 0 \\ 0 & 0 & 0 & 0 \\ 0 & 0 & 0 & 0 \\ \frac{t_s}{J_{fl}} & 0 & 0 & 0 \\ 0 & \frac{t_s}{J_{fr}} & 0 & 0 \\ 0 & 0 & \frac{t_s}{J_{rr}} & 0 \\ 0 & 0 & 0 & \frac{t_s}{J_{rl}} \end{bmatrix} \begin{bmatrix} -\alpha_{fl}K_B P_w(k) \\ -\alpha_{fr}K_B P_w(k) \\ T_{S,rr} - \alpha_{rr}K_B P_w(k) \\ T_{S,rl} - \alpha_{rl}K_B P_w(k) \end{bmatrix} \quad (4.3)$$

$$\mathbf{y} = \begin{bmatrix} 0 & 0 & 0 & 0 & 1 & 0 & 0 & 0 \\ 0 & 0 & 0 & 0 & 0 & 1 & 0 & 0 \\ 0 & 0 & 0 & 0 & 0 & 0 & 1 & 0 \\ 0 & 0 & 0 & 0 & 0 & 0 & 0 & 1 \end{bmatrix} \begin{bmatrix} f_{fl}(k) \\ f_{fr}(k) \\ f_{rr}(k) \\ f_{rl}(k) \\ \omega_{fl}(k) \\ \omega_{fr}(k) \\ \omega_{rr}(k) \\ \omega_{rl}(k) \end{bmatrix} \quad (4.4)$$

Examination of the pair (A,C) shows our system to be observable. Proceeding with the design of the observer, the estimator will take the form shown below:

$$\hat{\mathbf{x}}(\mathbf{k}+1) = A\hat{\mathbf{x}}(\mathbf{k}) + B\mathbf{u}(\mathbf{k}) + L(\mathbf{y}(\mathbf{k}) - C\hat{\mathbf{x}}(\mathbf{k})) \quad (4.5)$$

Based on trial and error, the gain matrix L was chosen as such:

$$L = \begin{bmatrix} -200 & 0 & 0 & 0 \\ 0 & -200 & 0 & 0 \\ 0 & 0 & -200 & 0 \\ 0 & 0 & 0 & -200 \\ 1 & 0 & 0 & 0 \\ 0 & 1 & 0 & 0 \\ 0 & 0 & 1 & 0 \\ 0 & 0 & 0 & 1 \end{bmatrix} \quad (4.6)$$

This set of gains places all of the eigenvalues of the closed loop estimator at $0.5025 \pm 0.0324i$. Since these eigenvalues are within the unit circle, the wheel speed estimates should converge to the actual wheel speeds.

4.1.1 Shaft Torque Observer Development

Whereas brake torque is estimated from equation 2.3, we have not described how shaft torque is determined. Here we will describe the observer [19] used to estimate shaft torque based on treatment of the drive shaft as a torsional spring. The differential equations describing the behavior of our two states, T_S and ω_{cr} , are given in equations 2.4 and 2.5. Putting our equations in state space form and discretizing:

$$\begin{bmatrix} \omega_{cr}(k+1) \\ T_S(k+1) \end{bmatrix} = \begin{bmatrix} 1 & 1 - \frac{R_d t_s}{J_{cr,i}} \\ 1 + KR_d t_s & 1 \end{bmatrix} \begin{bmatrix} \omega_{cr}(k) \\ T_S(k) \end{bmatrix} + \begin{bmatrix} \frac{t_s}{R_i J_{cr,i}} - \frac{1}{R_d R_i} & 0 \\ 0 & \frac{K t_s}{R_d} \end{bmatrix} \begin{bmatrix} T_t(k) \\ \omega_w(k) \end{bmatrix} \quad (4.7)$$

$$\mathbf{y} = \begin{bmatrix} 1 & 0 \end{bmatrix} \begin{bmatrix} \omega_{cr}(k) \\ T_S(k) \end{bmatrix} \quad (4.8)$$

Since the above pair (A,C) is observable, we can construct an observer of the form previously shown in equation 4.5. Experimentation resulted in choosing L as such:

$$\begin{bmatrix} 1 \\ 1 \end{bmatrix} \quad (4.9)$$

Depending on the what gear the vehicle is in, the observer's eigenvalues change. However, they always remain within the unit circle. It should be noted that the two states associated with this observer could be appended to the individual road force observer. In order to demonstrate the explicit effect of T_S on the road force estimates, this was not done.

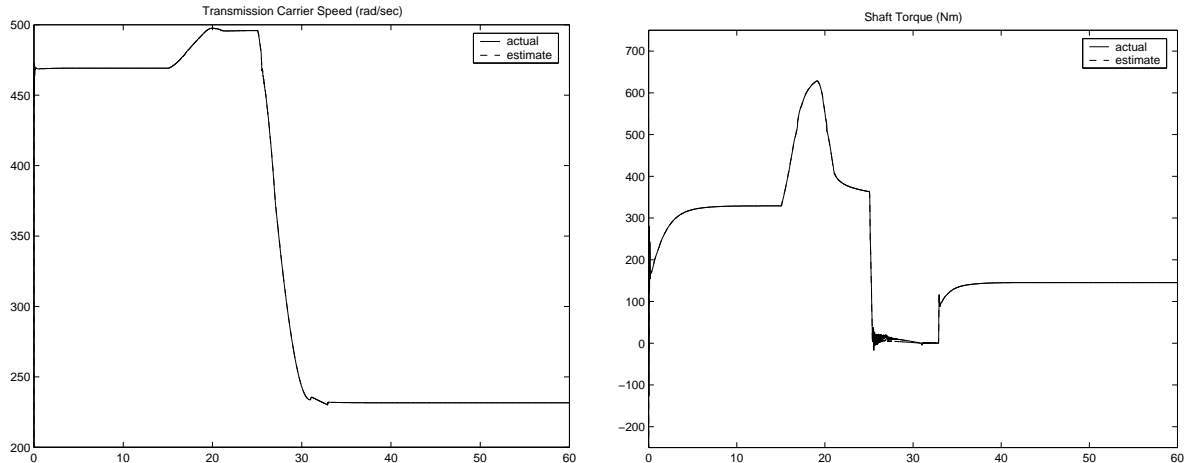


Figure 4.1: Shaft Torque Observer Performance with 50% Error in K

4.1.2 Shaft Torque Observer Simulation

The shaft torque observer performed very well when there was complete knowledge of all parameters. It also proved to be incredibly robust to errors in shaft stiffness, K . The estimate of T_S , where K is in error by 50% is shown in figure 4.1. You can hardly tell the difference between the actual and estimated states. This observer's primary weakness is its performance when turbine torque is not known exactly. There is an almost a one-to-one correspondence between error in the turbine torque estimate and error in the shaft torque estimate.

4.2 Individual Road Force Simulation

Simulations conducted using this observer showed very good performance under nominal conditions. The observer was also quite robust to error in the value of the wheel inertias. However, the performance of the observer degraded greatly when there were errors in wheel radius, shaft torque, or brake torque. Since our knowledge of wheel radius is fairly accurate, this is not a concern even under high acceleration maneuvers. However, determining the magnitude and distribution of the brake and shaft torque is a very difficult task.

The top graphs of figure 4.2 show the estimator's performance with an error of 50% in the brake torque gain. The lefthand side is the observer's nominal performance, while the righthand side is the observer's performance with error. There is an almost one-to-one correspondence between percent error in K_B and percent error in our force estimate.

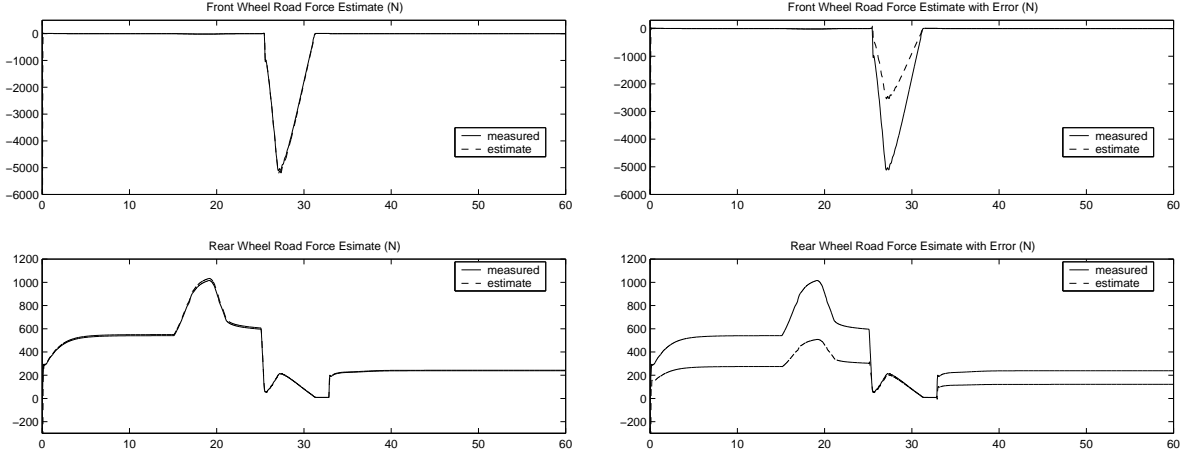


Figure 4.2: Individual Force Observer Performance With 50% Error in K_B and T_S

Errors in the shaft torque estimate result in performance degradation similar to that demonstrated for errors in K_B . This can be seen in the bottom graphs of figure 4.2.

4.3 Total Road Force Observer Development

This section outlines the design of the observer for estimating the sum of individual road forces. The approach of this observer is to estimate the total road force based on a model of the vehicle. As was the case for the individual force estimates, the total force estimate is assumed to be constant, and in this case is corrected based on our vehicle speed estimation error. The states for this observer are the same as those for the slip based controller:

$$\dot{V} = \frac{1}{M}(F - C_d V^2 - F_{rr}) \quad (4.10)$$

$$\dot{F} = 0 \quad (4.11)$$

We will essentially follow the same design procedure used for the individual force observer. By treating the drag and rolling resistance terms as inputs, we again have a set of linear differential equations. Putting these relations in a state space formulation and discretizing them, we end up with the following:

$$\begin{bmatrix} F(k+1) \\ V(k+1) \end{bmatrix} = \begin{bmatrix} 1 & 0 \\ \frac{t_s}{M} & 1 \end{bmatrix} \begin{bmatrix} F(k) \\ V(k) \end{bmatrix} + \begin{bmatrix} 0 & 0 \\ -\frac{t_s}{M} & -\frac{t_s}{M} \end{bmatrix} \begin{bmatrix} C_d V(k)^2 \\ F_{rr} \end{bmatrix} \quad (4.12)$$

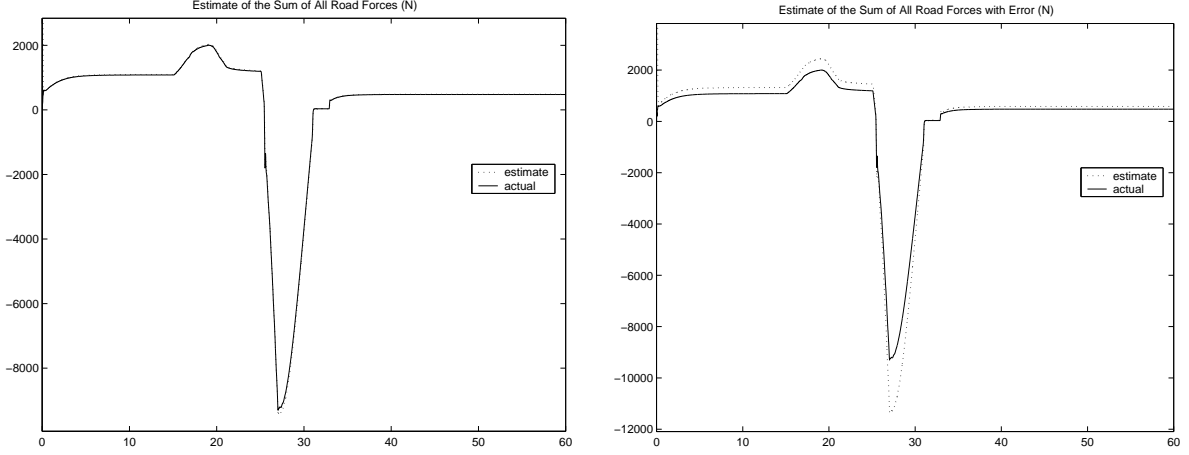


Figure 4.3: Total Force Observer Performance With 20% Error in M , C_d , and F_{rr}

$$\mathbf{y} = \begin{bmatrix} 0 & 1 \end{bmatrix} \begin{bmatrix} F(k) \\ V(k) \end{bmatrix} \quad (4.13)$$

From observation, one can see that the pair (A,C) is observable. This being true, we can now construct an observer of the form already shown in equation 4.5. Based on trial and error, the gain vector L was chosen as such:

$$\begin{bmatrix} 100000 \\ 1 \end{bmatrix} \quad (4.14)$$

This set of gains places the two eigenvalues of the observer at $0.5025 \pm 0.2557i$. This indicates that the velocity estimate error should converge to zero.

4.4 Total Road Force Simulation

The observer developed in the previous section performs very well when there is complete knowledge of all the parameters. The observer is however susceptible to error in vehicle mass, M , coefficient of drag, C_d , and rolling resistance, F_{rr} . Despite this, it should be noted that these quantities can be estimated a-priori, and are not likely to change significantly during operation. Furthermore, even if the drag and rolling resistance terms are in error, they are significantly smaller than the road force terms under braking or acceleration. The performance of the estimator with 20% error in M , C_d , and F_{rr} , can be seen in figure 4.3

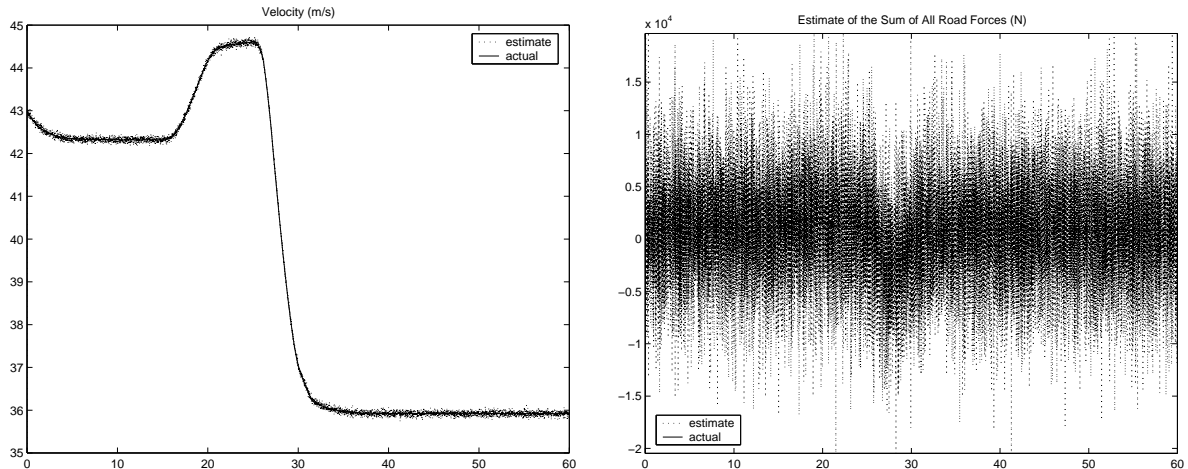


Figure 4.4: Total Force Observer Performance with Noise Contaminated Velocity Measurement

Aside from parameter uncertainty, this observer is also susceptible to error in the velocity measurement. Examination of figure 4.4 shows that the addition of a relatively small level of white noise to the velocity measurement has a very large adverse effect on the performance of the total force estimator. The actual total force trace is obscured by the noisy estimate, but is the same as in figure 4.3. This susceptibility seems to arise due to the very large gain associated with the total road force estimate.

4.5 Combined Road Force Estimator Simulation

In order to combine the results of the two individual observers, the relevant individual road force estimates are scaled to equal the total road force estimate. By relevant, it is meant that under braking, only braking wheels are scaled, and under acceleration, only driving wheels are scaled. One can see in the righthand side of figure 4.5 that the scaled individual estimates match the actual forces almost exactly, in spite of the error in K_B and T_S . Compare this result with the initial individual estimates shown in the lefthand graphs. Note that in these simulations the other parameters and measurements are known exactly, and that the percent error in K_B and T_S was distributed equally between the individual wheels.

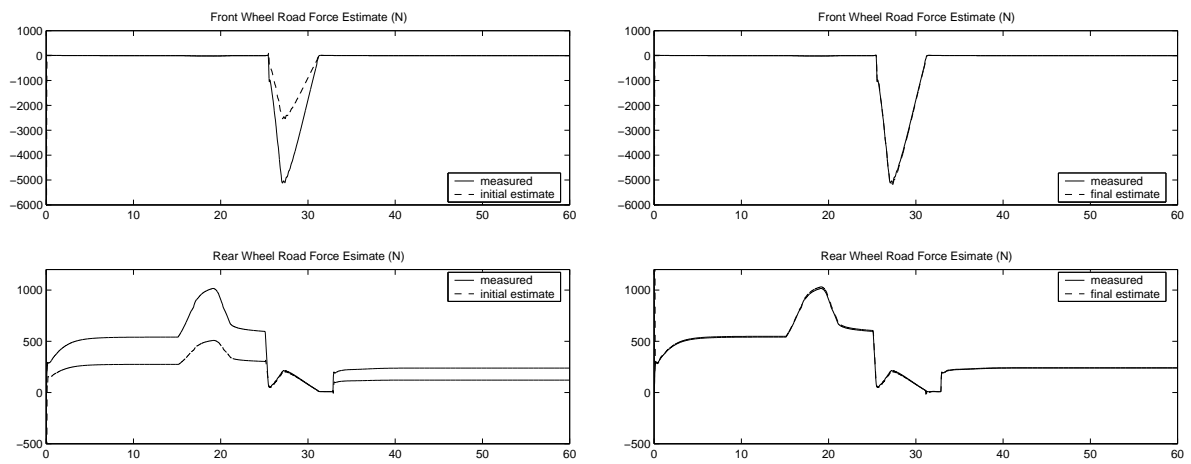


Figure 4.5: Combined Force Estimator Performance With 50% Error in K_B and T_S

Chapter 5

Experimental Testing

Despite the fact that extensive testing in simulation had been performed, experimental validation was still necessary. Simulation provided for a controlled environment for testing and development, and served to give a qualitative understanding of controller and observer performance. However, performance in a real world environment, which is of ultimate importance, still had to be assessed.

5.1 Experimental Setup

This section explains the hardware requirements as far as sensors and actuators that were used for the implementation and validation of the controller and observer designed in this paper.

5.1.1 Hardware for Implementation

All of the experimental work in this paper was performed on the Red Lincoln Towncar provided by California PATH. The control code for this vehicle is implemented in C on a Pentium processor running the QNX operating system. The actuators on the vehicle consist of a stepper motor on the throttle valve, and pump accumulator system that generates hydraulic pressure to actuate the vehicle's master cylinder. It should be noted that the brake actuator has been characterized as having a 30 msec pure time delay, as well as a first order lag of 20 msec.

Angular wheel speed is determined by hall effect type sensors on each wheel. Each sensor consists of a 50 tooth per revolution gear that generates current in a magnetic pick-up. The result is a sinusoidal signal whose frequency is proportional to angular speed. Furthermore, the amplitude of the signal increases as angular speed increases. This signal



Figure 5.1: Stock ABS Unit

is converted to three digital signals. One signal is optimized for low speed, one is optimized for high speed, and the other essentially averages over intervals of ten periods.

In our trials, vehicle velocity was determined from these wheel speeds. In general, under braking where all four wheels experience significant amounts of slip, this methodology will result in an incorrect estimate of vehicle velocity. To overcome this, we interfaced with the stock ABS unit of our test vehicle to close the valves on the brake lines leading to the vehicle's rear wheels. This combined with the fact that the car is rear wheel drive, guarantees that we will have at least two wheels that are not slipping at all times. For real world implementation, a velocity observer would have to be employed to determine the vehicle's longitudinal speed. This observer could combine information from wheel speeds, accelerometers, radar, and in the AHS environment, magnet counts.

Brake pressure at each wheel is determined from pressure transducers. For estimation of shaft torque, T_S , transmission carrier speed (ω_{cr}) is determined from a hall effect type sensor similar to that used for determination of the wheel speeds. This particular sensor has only three teeth per revolution. Estimation of T_S also requires sensing of transmission gear. Turbine torque T_t is determined from a look up table based on the ratio of speeds across the torque converter. Speed of the pump side of the converter is determined from engine speed, while speed of the turbine side of the converter is determined from transmission carrier speed, ω_{cr} . In third and fourth gear, the torque converter is locked, and T_t is equal to the torque generated by the engine. Engine torque is also determined by look up table, where the index is engine speed.

In all, implementation of the controller and observer outlined in this paper requires only inexpensive RPM sensors and at least one pressure transducer. The RPM sensors are

common to most vehicles produced today. The pressure transducer is less commonly found, but is widely used in general. Implementation of a velocity observer may require additional sensors.

5.1.2 Hardware for Validation

Validation of the road force observer is a difficult task for the same reason that the observer is necessary in the first place, it is all but impossible to sense road force directly.

One way that we were able to validate the observer was to look at the direct effect of road force on the dynamics of the vehicle. In other words, the forces acting on the vehicle are indicated by the vehicle's acceleration, where acceleration is determined from an accelerometer. Here the forces that act on the vehicle include wind drag and rolling resistance. We however have some idea of the magnitude of these two forces, and under braking and acceleration they are much smaller than the force from the road. Another obstacle is that the accelerometer indicates the sum of the road forces acting on the vehicle, while our observer's purpose is to estimate the individual road force at each wheel. Under braking, we can address this problem by again using the vehicle's ABS unit to brake with a single wheel at a time. Under acceleration, we have to assume that the road force generated by each drive wheel is equal. This is reasonable for straight line motion on a homogeneous surface.

Another means for validating our observer addresses the fact that the primary obstruction to building an accurate road force observer is the lack of good knowledge of brake and shaft torque. Therefore, if we can measure brake or shaft torque, we have a good idea of what the actual road force is. One of the brake rotors of our test vehicle has been instrumented with strain gauges for the direct purpose of measuring brake torque. Therefore, under braking, we have another means for verifying the road force estimate at one of the wheels. Under acceleration, we pretty much have to rely on the accelerometer for validation of the road force estimator.

5.2 Slip Estimation

For implementation of the slip based controller developed earlier, as well as any sort of road condition estimation scheme, the quantity of wheel slip must somehow be estimated. The essential methodology is to estimate wheel and vehicle speeds, then use the relation in equation 2.7 to calculate slip. This however is not as easy of a task as it may sound.



Figure 5.2: Torque Sensor

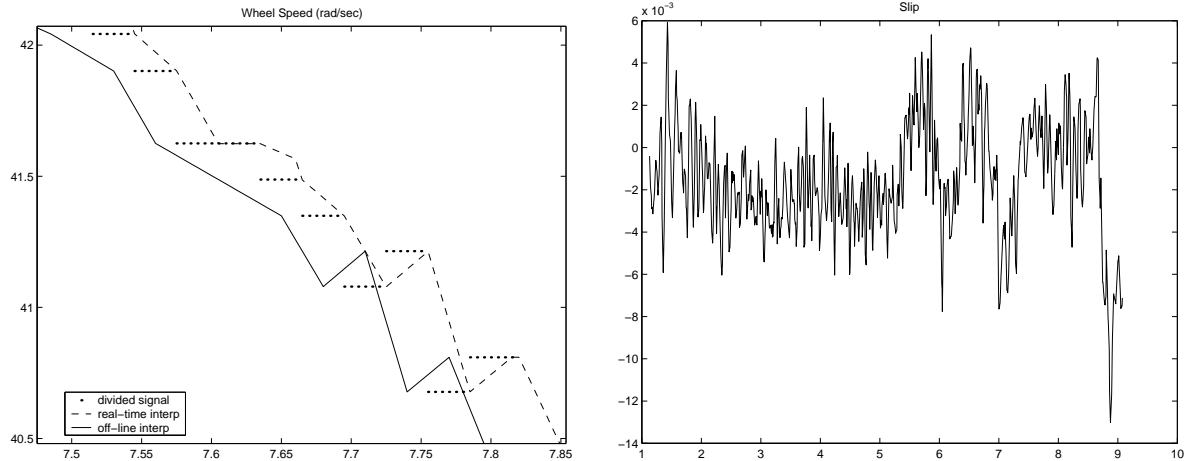


Figure 5.3: Wheel Speed and Slip Estimates

For our velocity estimates, it was determined that of the three wheel speed signals, the averaged signal would be best. The low speed signal drops out at $\sim 6 \frac{m}{s}$, so is not practical, and the high speed signal turned out to be too noisy. Since slip determination relies on a differential measurement of speed, noise is very detrimental. The averaged signal is much cleaner, but is updated ten times less frequently, resulting in wheel speed signal that has a staircase type shape. Since the averaged speed signal for one wheel is not necessarily averaged over the same time period as the other wheels, it is necessary to interpolate between each step. This interpolated 'signal,' will essentially have a lag of fifteen periods. This absolute lag is of little consequence compared to the relative shift between individual wheels, again because slip relies on a differential measurement. If conditioning can be performed off-line, this lag can be removed. The left half of figure 5.3 illustrates what the averaged and interpolated wheel speed signals look like. For a vehicle traveling ~ 30 mph, the interpolated wheel speed signal has a lag of ~ 50 msec.

As was mentioned earlier, for these trials vehicle velocity was determined from the angular velocity of the non-slipping wheels. This was possible since only the front wheels were used for braking. An example of a resulting estimate of wheel slip is shown in the right half of figure 5.3. Despite the noisy appearance of the signal, a correlation between road force and wheel slip can actually be detected. Refer to [14] for a more indepth account of slip estimation.

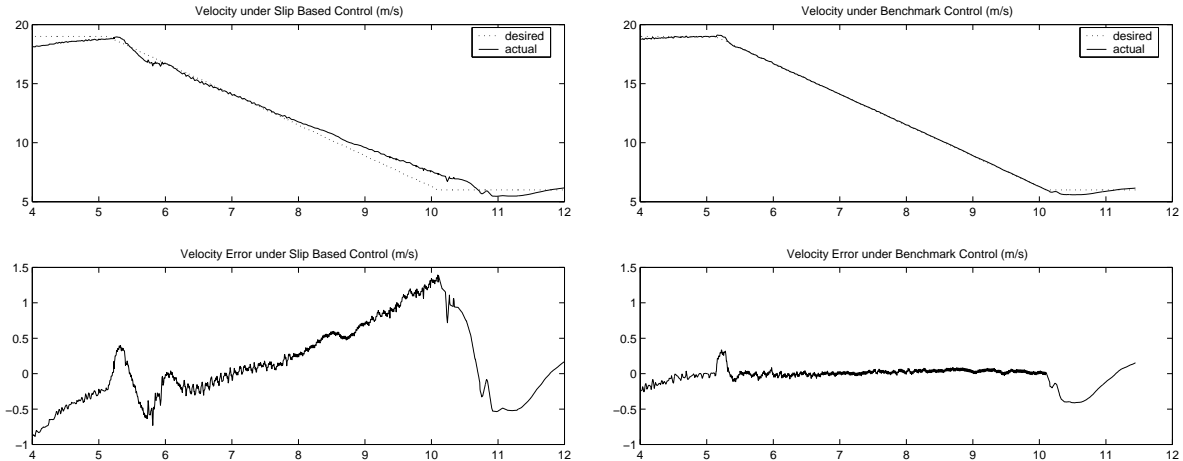


Figure 5.4: Slip Based and Benchmark Controller Experimental Performance

5.3 Slip Based Control

In addition to being tested in simulation, the slip based and benchmark controllers developed earlier in this paper were evaluated on an actual test vehicle. A representation of the results of this testing are shown in figure 5.4. From observation one can see that the error under the benchmark controller, on the right, is much better than the error under the slip based controller shown on the left. Some insight into the performance of each controller can be gained from examination of the control signals produced in each case.

The control effort required by each controller can be seen in figure 5.5. Under slip based control, shown on the left, the desired brake pressure is much more oscillatory than under benchmark control. From the simulations performed earlier, it is thought that this chatter is caused by the filter and slip dynamics associated with the second surface of the slip based controller.

5.4 Road Force Observation

Demonstration of the road force observer will essentially be delivered in two steps. The first step will show estimator results where all calculations were performed off-line. This will allow us to evaluate the estimator without regard to any of the introduced time lags. The second step of evaluation will then look at the results where all calculations were performed on the vehicle in real time. It should be noted that even off-line operation of the observer can be of use in an AHS environment. This is the case since in an AHS, information can be shared among different vehicles, hence, the road force estimate doesn't

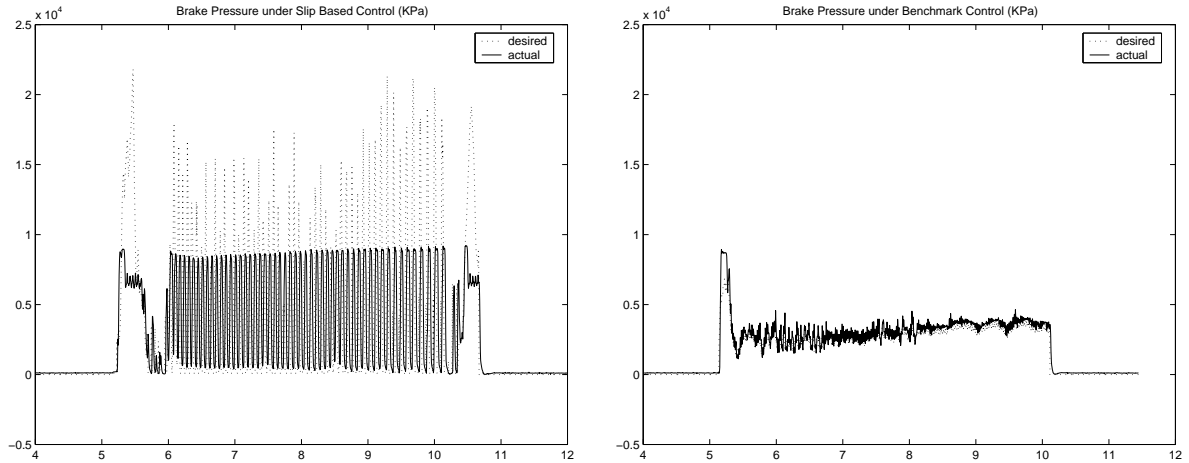


Figure 5.5: Slip Based and Benchmark Controller Control Effort

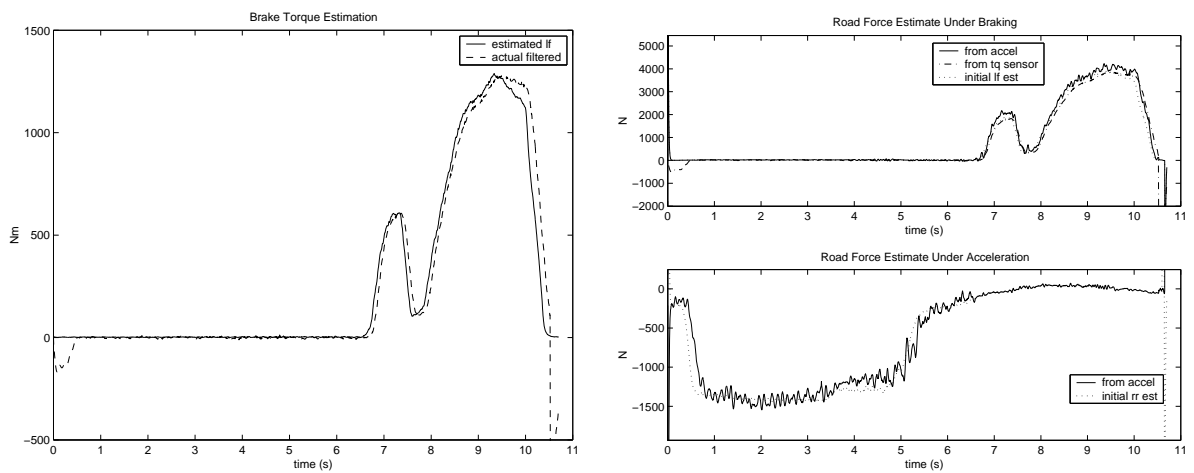


Figure 5.6: Off-line Individual Road Force Observer Performance

have to be available in real-time to be useful.

5.4.1 Off-line Individual Road Force Observer

Figure 5.6 shows the observer's performance for one run. Noting in the left hand graph, the brake torque parameter K_B has been chosen such that the brake torque estimate based on brake pressure is in agreement with the reading from the brake torque sensor. There is a small amount of lag between the brake pressure trace and the resulting brake torque generation. Under these conditions, the observer's performance indicated in the right half graphs is very good.

Figure 5.7 shows another set of results from the individual road force observer. This figure illustrates the limitations of this estimator. Here the brake torque parameter

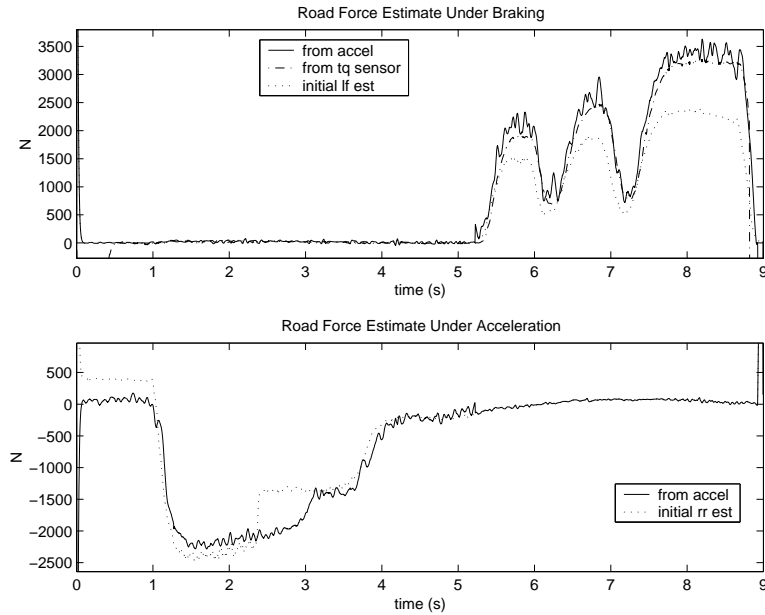


Figure 5.7: Individual Road Force Observer Weaknesses

K_B is in error, which causes the estimated road force under braking to be in error. Under acceleration, one can see a large error in the force estimate at ~ 2.3 sec. This time index corresponds to a gear shift. This error is likely attributable to error in the shaft torque estimate. Since we have no way of measuring shaft torque directly, an error in its estimation is only evident in its ultimate effect on the road force estimate. This error in shaft torque estimate seems to indicate a deficiency in the turbine and/or engine torque maps. Another deficiency in these maps is that they seem to consistently overestimate the torque being generated, especially under engine braking. This would account for the disparity between the road force indicated by the accelerometer and the torque sensor. Since the accelerometer is only an indication of the total road force, if the estimate of engine braking is smaller than it should be, the road force at the braking wheel estimated by the accelerometer will be larger than that indicated by the torque sensor.

5.4.2 Off-line Total Road Force Observer

The performance of the off-line total road force observer can be seen in figure 5.8. Overall there is good agreement between the estimate and total road force indicated by the vehicle's accelerometer. The noise associated with the estimate seems to indicate error in the velocity measurement. This noise can be decreased by lowering the observer gain. This however results in degraded tracking. For off-line operation, the noise isn't much of an issue

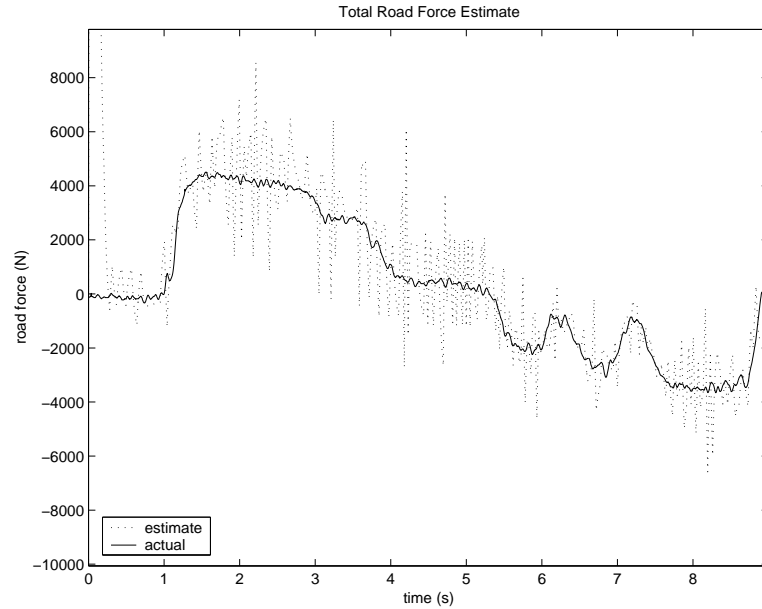


Figure 5.8: Off-line Total Road Force Observer Performance

since the estimate can be heavily filtered forward and backward in time to avoid any time lag.

5.4.3 Off-line Combined Road Force Estimator

The left half of figure 5.9 shows the results of the combined force estimator for the same run that was used in figure 5.7. The combination of the individual and total road force estimates can be seen to have corrected for the brake and shaft torque errors quite well. The only real deficiency that occurs is again a result of the engine braking estimate being too small. This problem indicates the primary weakness of this approach, if we don't know how the error is distributed between the individual wheels, it can't be corrected for.

So far all the runs that have been made have involved braking with only one wheel so that validation with the accelerometer could be performed. The results displayed in the right half graphs of figure 5.9 are for a run where both front wheels were used for braking. The estimated road forces match those indicated from the vehicle accelerometer and torque sensor quite well. This result gives us some confidence that the error in the brake torque estimate is indeed equally distributed.

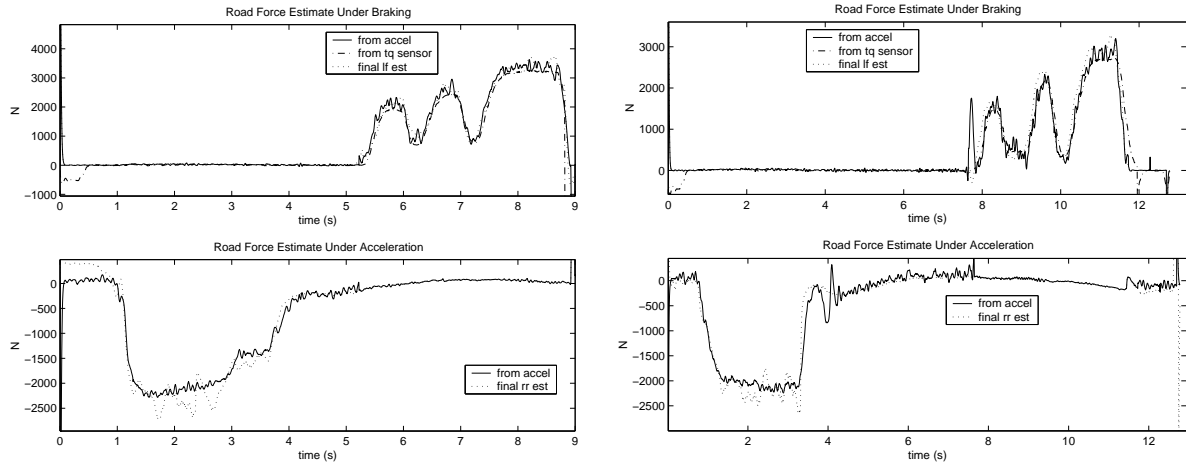


Figure 5.9: Off-line Combined Road Force Estimator Performance

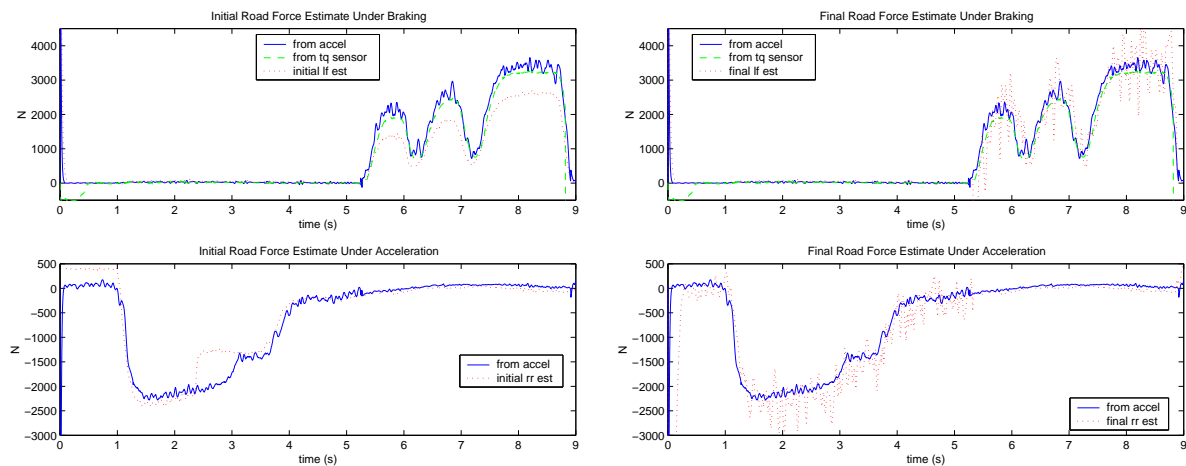


Figure 5.10: Real-time Combined Road Force Estimator Performance

5.4.4 Real-time Combined Road Force Estimator

There are essentially two problems associated with real-time operation of this observer. One is the time lag associated with the wheel speed measurements, while the other is the noise associated with the total road force estimate. With the total road force estimate, the basic tradeoff is between noise level and time lag. Figure 5.10 shows the real-time performance of the estimator. Again the combined estimator corrects for the deficiencies apparent in the left half graphs, however, you will notice that the estimates are noisier and have more time lag than the off-line estimates in figure 5.9. In this case, a first order filter with time constant of 25 msec was used to clean up the total force estimate.

One final indication of the real-time performance of the estimator can be seen in

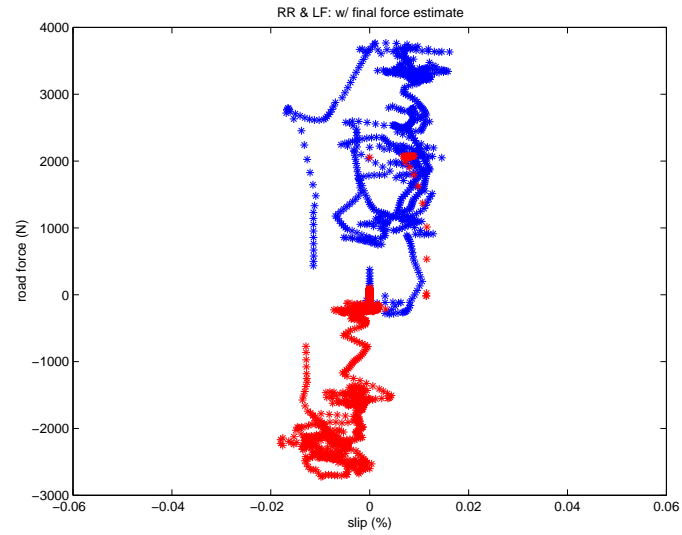


Figure 5.11: Correlation Between Real-Time Slip and Road Force Estimates

figure 5.11. This figure demonstrates the correlation between the real-time slip and road force estimates. Despite the noise and lag associated with each, a very strong linear trend can be observed.

Chapter 6

Conclusions

6.1 Slip Based Controller Summary

This paper developed and evaluated a non-linear brake controller that accounted for wheel slip in its derivation. The performance of this controller was assessed with respect to a controller that employs a limited slip rolling condition. Simulation work demonstrated that with perfect knowledge and an ideal actuator, the new controller offered improvement in velocity and spacing error over the benchmark controller. It however was also shown that the addition of measurement uncertainty and actuator delay increased the level of chatter associated with the controllers, with the slip based controller being affected in particular. To address this, the gain associated with the second surface had to be decreased, thereby negating the gains that the slip based controller had initially provided. Further simulation showed that the filter constant associated with $F_{des, filt}$ and the characteristic slip curve of the road being traveled upon both affected the level of chatter. These results seem to indicate that the additional chatter associated with the slip based controller is caused by the added filter and slip dynamics of the second surface. Experimental results demonstrated that this chatter so degraded performance that the tracking provided by the slip based controller was appreciably worse than the benchmark controller.

An adaptive version of the slip based controller was also developed to estimate the brake torque parameter K_B . This adaptation algorithm worked quite well in simulation, but relies on actual employment of the controller.

From simulation and experimental results it was concluded that any benefits derived from the slip based controller arose because it used an extra surface in its implementation. The limited slip assumption seemed to minimally affect performance for a couple of reasons. The primary reason being that the first error surface effectively closed

the loop around, and corrected for any errors associated with the limited slip assumption. This combined with the facts that any braking maneuver is going to be relatively constant, sampling times are going to be relatively small, and slip is always going to remain below a level of $\sim 15\%$, results in the contribution of the limited slip assumption being quite small. The reason the level of slip is going to remain below $\sim 15\%$, is because the peak of the slip curve of most any road condition will be below that level. Since the peak is where the largest road force is supplied, and because a wheel will lock up if that peak is surpassed, it is reasonable to assume that any control strategy would keep the level of slip below this. It should be noted that neither controller keeps the vehicle in this region of operation. Under emergency conditions another level of control, like ABS, would be necessary.

Overall it was determined that existing control strategies are quite robust, even in the face of wheel slip. The slip based controller presented here could possibly offer benefits in an application where accurate slip and road condition information were available, and an actuator was available that had minimal delay associated with it. Since slip and road condition are difficult to obtain, and an improved actuator would likely have to be an impractical electrical alternative, it is recommended that existing control strategies continue to be employed.

6.2 Road Force Estimator Summary

Despite the limitations of the slip based controller, the road force estimator that was developed could still be quite useful. In the context of this paper, the estimator was developed to be part of a scheme to identify road condition based on the relationship between slip and normalized road force. Knowledge of road condition is useful to other applications aside from a slip based controller. In general, knowledge of road condition is of use in any automated vehicle control application where it is desired to operate within some performance envelope.

Successful performance of the estimator was demonstrated in simulation and in operation on an actual vehicle. The primary limitation of the estimator was shown to arise if the distribution of brake or shaft torque between individual wheels was unknown. It was also however demonstrated for the front two wheels that it is reasonable to assume that the distribution of brake torque remains constant, even if the overall brake torque gain K_B changes. Two problems that arise in real-time operation of the estimator are that the estimates suffer a time lag and are noisier. The lag and noise however are relatively minor. Furthermore, in an AHS application where information is shared between many vehicles,

the estimator could be of benefit even if all the calculations were performed off-line.

6.3 Future Work

In regards to the slip based controller, a next step would be to try and quantify the controller's oscillatory behavior, perhaps in the form of stability margins. This could maybe offer some insight into what causes the oscillation, and how it could be overcome. Furthermore, it would be interesting to investigate the effect of the limited slip assumption in the operation of a platoon of vehicles, as opposed to the single vehicles that were looked at here. An even further step would be to develop the next higher level of control. In other words, future work can be done on platoon control and vehicle coordination in emergency situations. The objective being to develop strategies that bring platoons of vehicles to a stop as quickly and safely as possible.

The next step associated with the road force observer would be to develop a scheme that actually classifies road condition based on slip and road force information. Some existing strategies accomplished this by looking at the slope of the slip curve near origin [5], or by matching the parameters of various tire models [11] [13] [15]. The road force estimator could also be applied to a vehicle dynamic control (VDC) system. The aim of this type of system being to keep a vehicle in its stable region of operation, in other words, to prevent a vehicle from skidding out of control.

In relation to the previous areas of work mentioned, a necessary development would be the design and implementation of a velocity observer. As was noted, under braking all wheels experience significant levels of slip, hence vehicle longitudinal velocity cannot be determined from wheel or transmission speed. Possible approaches include combining information from wheel speeds, accelerometers, radar, or in the AHS environment, magnet counts [4] [7]. Along these lines, it seems improved wheel speed signals could be acquired if new sensors were used in place of the decade old inductive sensors currently employed.

Bibliography

- [1] Bakker, Egbert, and Hans Pacejka, *A New Tire Model with an Application in Vehicle Dynamics Studies*, SAE Paper 890087, 1987, pp 101-13.
- [2] Breuer, B., Eichorn, U., and J. Roth, "Measurement of Tyre/Road Friction Ahead of the Car and Inside the Tyre," *Proceedings of the International Symposium on Advanced Vehicle Control*, 1992, pp 347-53.
- [3] Broucke, Mireille and Pravin Varaiya, "The Automated Highway System: A Transportation Technology for the 21st Century," *International Federation of Automatic Control World Congress*, 1996.
- [4] Daiß, A., and U. Kiencke, "Estimation of Vehicle Speed Fuzzy Estimation in Comparison with Kalman-Filtering," *IEEE paper*, 1995, pp 281-4.
- [5] Gustafsson, F., "Monitoring Tire-Road Friction using the Wheel Slip," *IEEE Control Systems Magazine*, vol 18, (no. 4), August 1998, pp 42-9.
- [6] Holzwarth, F., and U. Eichorn, "Non-contact Sensors for Road Conditions," *Sensors and Actuators*, June-Aug. 1993, pp 121-7.
- [7] Kobayashi, K., Cheok, Ka.C., and K. Watanabe, "Estimation of Absolute Vehicle Speed using Fuzzy Logic Rule-Based Kalman Filter," *Proceedings of the American Controls Conference*, 1995, pp 3086-90.
- [8] Lim, Edward M., *Lateral and Longitudinal Vehicle Control Coupling in the Automated Highway System*, M.S. Thesis, University of California at Berkeley, 1998.
- [9] Maciuca, Dragos B., *Nonlinear Robust and Adaptive Control with Application to Brake Control for Automated Highway Systems*, Ph.D. Dissertation, University of California at Berkeley, 1994.

- [10] Maciucă, Dragos B., and J.K. Hedrick, "Brake Dynamics Effect on AHS Lane Capacity," *Systems and Issues in ITS (SP-1106)*, SAE Paper 951929, 1995.
- [11] Kiencke, U., and A. Daiß, "Estimation of Tyre Friction for Enhanced ABS-Systems," *Proceedings of the International Symposium on Vehicle Control*, 1994, pp 515-20.
- [12] McMahon, D.H., *Robust Nonlinear Control of Uncertain Systems: An Application to Intelligent Vehicle Highway Systems (IVHS)*, Ph.D. Dissertation, University of California at Berkeley, 1994.
- [13] Pal, C., Hagiwara, I., Morishita, S., and H. Inoue. "Application of Neural Networks in Real Time Identification of Dynamic Structural Response and Prediction of Road-Friction Coefficient μ from Steady State Automobile Response," *Proceedings of the International Symposium on Advanced Vehicle Control*, 1994, pp 527-32.
- [14] Petersson, N., and M. Santesson, "Experimental Slip-based Road Condition Estimation," M.S. Thesis, Lund Institute of Technology, February 2000.
- [15] Ray, Laura R., "Experimental Determination of Tire Forces and Road Friction," *Proceedings of the American Control Conference*, 1998, pp 1843-47.
- [16] Swaroop, D., *String Stability of Interconnected Systems: An Application to Platooning in Automated Highway Systems*, Ph.D. Dissertation, University of California at Berkeley, 1994.
- [17] Swaroop, D., J.K. Hedrick, P. Yip, and J.C. Gerdes, "Dynamic Surface Control for a class of Nonlinear Systems," *submitted to IEEE Transactions on Automated Control*, 1999.
- [18] Uno, T., Sakai, Y., Takagi, J., and T. Yamashita, "Road Surface Recognition Method using Optical Spatial Filtering," *Proceedings of the International Symposium on Advanced Vehicle Control*, 1994, pp 509-15.
- [19] Yi, Kyongsu and Taeyoung Jeoung, "Road Friction Estimation Using Wheel Speed Sensors," *5th World Congress on Intelligent Transportation Systems*, 1998.
- [20] Zabat, Michael, Nick Stabile, Stefano Frascaroli, and Frederick Browand, *The aerodynamic performance of platoons: Final Report*, Technical Report UCB-ITS-PRR-95-35, California Path, 1995.

Appendix A

Nomenclature

a	=	vehicle longitudinal acceleration
a_{des}	=	desired vehicle longitudinal acceleration
C_d	=	longitudinal drag coefficient
f	=	individual longitudinal road force acting at a wheel
F	=	total longitudinal road force acting on the vehicle
F_{des}	=	desired total longitudinal road force
$F_{des,flt}$	=	filtered approximation of F_{des}
F_N	=	tire normal force
F_{rr}	=	rolling resistance
J	=	tire moment of inertia
$J_{cr,i}$	=	transmission carrier inertial in i^{th} gear
K	=	drive shaft torsional stiffness
K_B	=	gain between brake pressure and the resulting brake torque
M	=	vehicle mass
P_w	=	brake pressure at the wheel
r	=	tire radius
R_d	=	differential gear ratio
R_i	=	i^{th} transmission gear ratio
s	=	longitudinal tire slip ratio
T_B	=	brake torque

T_S = drive shaft torque

V = vehicle longitudinal velocity

α = percentage of the overall brake torque distributed to a particular wheel

ε = longitudinal spacing error

μ = road coefficient of friction

ω = tire angular velocity

ω_{cr} = transmission carrier speed